AD-A188 853 A NUMERICAL ANALYSIS OF THE DYNAMICS OF PRIZ OPERATION (U) AIR FORCE INST OF TECH WRIGHT-PATTERSON AFB OH SCHOOL OF ENGINEERING D A CUSHING JUL 87 1/1

UNCLASSIFIED AFIT/GEP/ENP/87J-2 F/G 20/6 NL

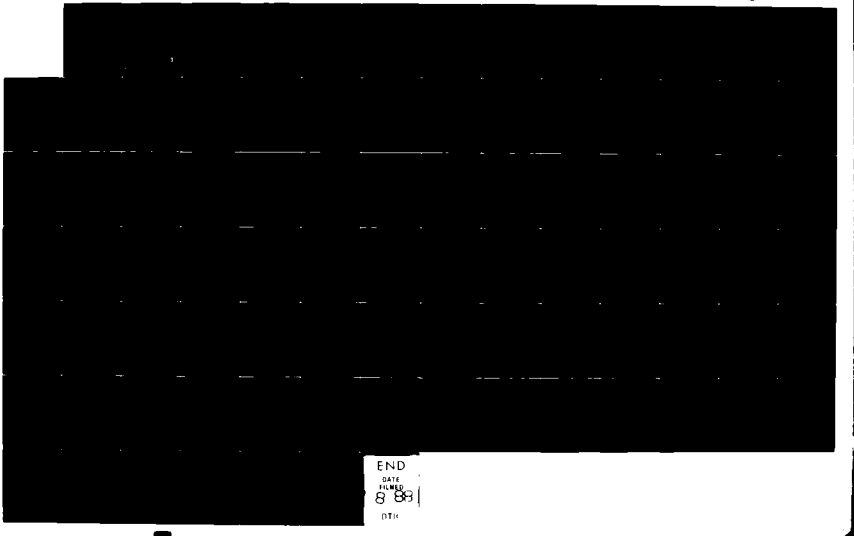

END

DATE FILMED

8 88

DTIC

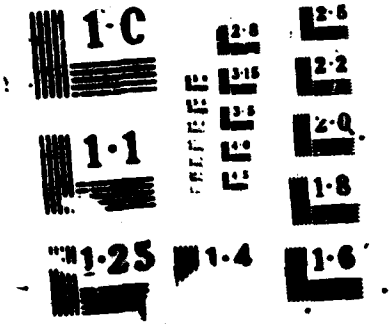
1·C
1·1
1·25
2·8
3·15
2·5
2·2
2·0
1·8
1·4
1·6

AD-A188 853

DTIC FILE COPY

A NUMERICAL ANALYSIS OF THE DYNAMICS OF PRIZ OPERATION

THESIS

David A. Cushing
First Lieutenant, USAF

AFIT/GEP/ENP/87D-8

DTIC ELECTE FEB 10 1988 S D E

DEPARTMENT OF THE AIR FORCE
AIR UNIVERSITY
AIR FORCE INSTITUTE OF TECHNOLOGY

Wright-Patterson Air Force Base, Ohio

This document has been approved for public release and sale; its distribution is unlimited.

88 2 4 048

A NUMERICAL ANALYSIS OF THE DYNAMICS OF PRIZ OPERATION

THESIS

David A. Cushing
First Lieutenant, USAF

AFIT/GEP/ENP/87D-3

J-1

DTIC ELECTE

Approved for public release; distribution unlimited

UNCLASSIFIED
SECURITY CLASSIFICATION OF THIS PAGE

REPORT DOCUMENTATION PAGE

Form Approved
OMB No. 0704-0188

1a. REPORT SECURITY CLASSIFICATION UNCLASSIFIED	1b. RESTRICTIVE MARKINGS
2a. SECURITY CLASSIFICATION AUTHORITY	3. DISTRIBUTION/AVAILABILITY OF REPORT Approved for public release; distribution unlimited.
2b. DECLASSIFICATION/DOWNGRADING SCHEDULE	
4. PERFORMING ORGANIZATION REPORT NUMBER(S) AFIT/GEP/ENP/87J-1	5. MONITORING ORGANIZATION REPORT NUMBER(S)
6a. NAME OF PERFORMING ORGANIZATION School of Engineering 6b. OFFICE SYMBOL (If applicable) AFIT/ENP	7a. NAME OF MONITORING ORGANIZATION
6c. ADDRESS (City, State, and ZIP Code) Air Force Institute of Technology Wright-Patterson AFB, Ohio 45433	7b. ADDRESS (City, State, and ZIP Code)
8a. NAME OF FUNDING/SPONSORING ORGANIZATION 8b. OFFICE SYMBOL (If applicable)	9. PROCUREMENT INSTRUMENT IDENTIFICATION NUMBER
8c. ADDRESS (City, State, and ZIP Code)	10. SOURCE OF FUNDING NUMBERS PROGRAM ELEMENT NO. / PROJECT NO. / TASK NO / WORK UNIT ACCESSION NO.

11. TITLE (Include Security Classification)

A NUMERICAL ANALYSIS OF THE DYNAMICS OF PRIZ OPERATION (Unclas.)

12. PERSONAL AUTHOR(S)

David A. Cushing, B.S., 1Lt, USAF

13a. TYPE OF REPORT	13b. TIME COVERED	14. DATE OF REPORT (Year, Month, Day)	15. PAGE COUNT
MS Thesis	FROM _____ TO _____	1987 July	86

16. SUPPLEMENTARY NOTATION

17. COSATI CODES			18. SUBJECT TERMS (Continue on reverse if necessary and identify by block number)
FIELD	GROUP	SUB-GROUP	
20	06		PRIZ, Conducting PRIZ, Spatial Light Modulator, BSO, Dynamic Image Selection

19. ABSTRACT (Continue on reverse if necessary and identify by block number)

Thesis Chairman: Dr. William F. Bailey

31 Aug 87
...d Professional Development
...nstitute of Technology (...)
Wright-Patterson AFB, Ohio

A numerical computer model of the PRIZ electro-optic spatial light modulator is presented. Guided by the earlier work of Astratov, this model involves differencing the longitudinal spatial derivative and using a numerical integration technique to solve the time derivative. The model is validated by comparing the numerical results with the analytical theory developed by Bryskin. Bryskin has spent several years developing a theoretical analysis of the PRIZ device. The primary elements were reviewed and in selected instances, extended. Differences are noted and possible explanations are offered. Comparisons are also made with experimental results. Finally, the model is extended to solve for the integrated transverse field in the case of a simple spot. (Continued on back)

20. DISTRIBUTION/AVAILABILITY OF ABSTRACT	21. ABSTRACT SECURITY CLASSIFICATION
☒ UNCLASSIFIED/UNLIMITED ☐ SAME AS RPT. ☐ DTIC USERS	UNCLASSIFIED

22a. NAME OF RESPONSIBLE INDIVIDUAL	22b. TELEPHONE (Include Area Code)	22c. OFFICE SYMBOL
Dr. William F. Bailey	513-225-2012	AFIT/ENP

DD Form 1473, JUN 86 — Previous editions are obsolete. — SECURITY CLASSIFICATION OF THIS PAGE

UNCLASSIFIED

AFIT/GEP/ENP/87J-1

A NUMERICAL ANALYSIS OF THE DYNAMICS OF PRIZ OPERATION

THESIS

Presented to the Faculty of the School of Engineering
of the Air Force Institute of Technology
Air University
In Partial Fulfillment of the
Requirements for the Degree of
Master of Science in Engineering Physics

DTIC COPY INSPECTED

Accession For
NTIS GRA&I
DTIC TAB
Unannounced
Justification
By
Distribution/
Availability Codes
Dist | Avail and/or Special
A-1

David A. Cushing, B.S.
First Lieutenant, USAF

July 1987

Approved for public release; distribution unlimited

Preface

This thesis is in response to the continued interest in the PRIZ device at AFIT. Some experimental work has been done in the United States, primarily at AFIT, but the majority of the theoretical work to date has been in the Soviet Union. A review of the theoretical work done in the Soviet Union is presented here, and further development of the theory is presented. A numerical model of the PRIZ device is presented and compared with theory and experiment.

My sincerest thanks go to Dr. Bailey for his guiding hand and patience throughout this project. Perhaps he will be rewarded with a competent researcher. Dr. Luke and Major Lupo deserve special mention for providing their inputs into this project as well.

Special thanks is due Major Lupo, whose graphical subroutines added immeasurably to this thesis.

Finally, I would like to thank my family, who, although their support was of a long distance nature, always deserve at least some of the credit for anything I do.

David A. Cushing

TABLE OF CONTENTS

List of Figures

Notation

Symbol		1st Appearance
α	absorption coefficient	eq 2.7
A_r	area of PRIZ crystal	pg 34
d_o	crystal thickness	eq 1.1
e	modulus of electron charge	eq 2.1
ϵ	dielectric constant of material	eq 3.6
ϵ_o	permittivity of free space	eq 3.6
ϵ'	total permittivity of material	eq 2.16
E	total z component of electric field	eq 2.9
$\mathcal{E}$	ratio of total electric field and applied electric field	eq 2.20
E_o	externally applied electric field	eq 2.4
E_t'	longitudinally integrated transverse electric field	eq 1.2
f_o	quantum efficiency of material	eq 2.14
g	rate of electron excitation into the conduction band	eq 2.2
γ	ratio between drift length and absorption length	eq 2.18
Γ	Electric vector phase difference	eq 1.1
$h\nu$	photon energy	eq 2.14
I	intensity of write beam in W/m^2	eq 2.14
j	current density	eq 2.1
kT	electron temperature in eV	eq 2.4
ℓ	electron drift length in applied electric field	eq 2.19
λ	wavelength of light	eq 1.1
μ	electron mobility	eq 2.4

n	density of electrons in conduction band	eq 2.1
n_o	normalization density	eq 2.16
n_-	density of negatively charged traps	eq 2.1
n_+	density of donor sites	eq 2.1
n_t	density of traps	eq 2.3
n'	index of refraction	eq 1.1
φ	potential due to internal charge	eq 2.4
Q	surface charge across device	eq 2.27
σ	area charge density	eq 3.6
r_{63}	electro-optic coefficient	eq 1.1
ρ	spatial charge number density	eq 2.17
ρ_f	spatial charge number density due to fixed carriers only	eq 3.2
t	time in seconds	eq 2.1
t_d	time for image to decay	eq 5.1
t_o	temporal boundary between linear and nonlinear regimes	eq 2.15
τ_t	electron lifetime in conduction band	eq 2.8
τ_{th}	thermal ionization time of shallow traps	eq 2.3
V	applied potential	eq 2.35
ϕ_d	recombination time at donor sites	eq 2.2
ϕ_t	recombination time at deep traps	eq 2.3
y	coordinate transverse to write beam	eq 4.1
z	coordinate parallel to write beam	eq 2.7
z_o	interface between positive and negative space charge regions	eq 2.19

Abstract

A numerical computer model of the PRIZ electro-optic spatial light modulator is presented. Guided by the earlier work of Astratov, this model involves differencing the longitudinal spatial derivative and using a numerical integration technique to solve the time derivative. The model is validated by comparing the numerical results with the analytical theory developed by Bryskin. Bryskin has spent several years developing a theoretical analysis of the PRIZ device (ref. 10 and ref. 9). The primary elements were reviewed and in selected instances, extended. Differences are noted and possible explanations are offered. Comparisons are also made with experimental results. Finally, the model is extended to solve for the integrated transverse electric field in the case of the simple spot. The integrated field is found to have nearly a 1/r dependence. The solution for a simple spot is used to explain the "edge-enhancement" effect of a simple spot reported by Shields. The damage to the PRIZ is then briefly discussed.

Chapter I

PRIZ is a Russian acronym for a spatial light modulator. The PRIZ device is a simple modulator capable of optical image storage and even dynamic imaging with edge enhancement. Potential applications in the areas of optical computing, optical signal processing, and image pattern recognition (12:1) have stimulated significant research and development efforts on these devices. Petrov and Bryskin (ref. 10 and ref. 16) have led a concerted and sustained Soviet developmental effort which has provided experimental data on the PRIZ. They have formed a theoretical basis for understanding the principles of operation and have characterized the modes of operation. Experimental results consist chiefly of longitudinal electric field measurements in various modes. The theoretical development has provided analytic expressions for certain limiting cases, and highlighted two operational regimes of the device.

Recently, Shields and Luke (ref. 17) constructed and tested a PRIZ. Their studies (the first outside of the Soviet Union), confirmed those capabilities reported by the Soviets, and reproduced many of their results. In a subsequent study, Nilius and Luke (ref. 12) reported on the memory capability of the device. Anderson and Luke (2:3) later noted that under typical "write beam" conditions, the crystal can experience significant damage. This damage can

lead to modification and degradation in the PRIZ operating characteristics; thus severely restricting development.

Problem Statement

A generalized theoretical analysis was initiated to parameterize the operating regime of the PRIZ devices. Previous analyses provided guideposts in the validation process; but were of limited or uncertain general utility. They often employed unrealistic or restrictive assumptions which were inconsistent with the conditions encountered for realistic device applications. The generalized approach, however, was based on a direct numerical integration of the rate equations governing PRIZ operation. The kinetic processes, either in number, spatial dependence or type, were not restrictive to the method employed. Employing this approach, the temporal and spatial distribution of charges and the internal fields have been characterized under a broad range of excitation conditions. Comparisons have been made with existing analytic solutions, and scaling laws have been identified.

PRIZ Fabrication and Operation

The PRIZ is most often built of the photo-refractive crystal, $Bi_{12}SiO_{20}$ (BSO) (17:1). Some experiments relating to the PRIZ have been performed with the crystal, $Bi_{12}GeO_{20}$ (3:1585). These crystals form the basis for two types of

devices: the 'conducting' PRIZ and the 'standard' PRIZ. These are pictured in Figure 1.1. The 'conducting' PRIZ consists of a (111) or (110) cut BSO crystal to which transparent electrodes are applied. The 'standard' PRIZ consists of the same BSO crystal; however in this design the crystal is sheathed in dielectric material before the application of the transparent electrodes.

The external electric field is oriented parallel to the incoming write beam. The write beam typically deposits anywhere from 1 to 250 μJ on the device. The wavelengths used are in the visible range, so the device can be viewed without sophisticated optical equipment. The write beam photo-excites electrons from donor sites into shallow traps, between 0.6 eV and 0.3 eV (10:878). From the shallow traps, electrons can be thermally excited into the conduction band. Write beams composed of more energetic photons can excite electrons directly into the conduction band. The electrons in the conduction band drift due to the external applied field and are trapped in deeper traps, at 1.3 eV and 1.25 eV (15:3686). The trapped electrons, the now positively charged donor sites, and the still mobile electrons create a non-uniform charge distribution in the crystal. This charge distribution acts to set up a new internal field with transverse components.

Using a polarizer before the illuminated face and an analyzer after the dark face, Figure 1.2, a read beam can be

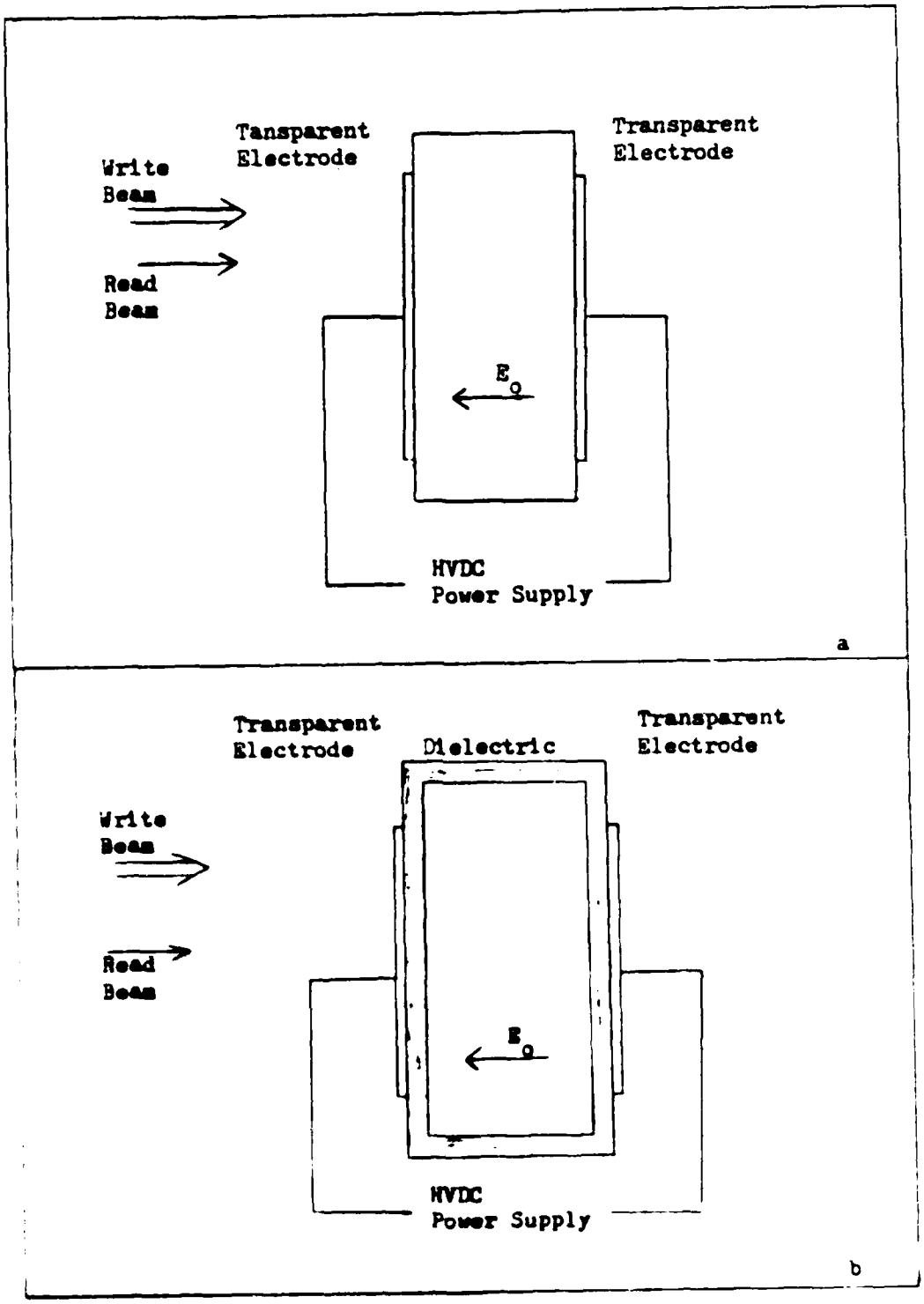

Figure [illegible] ...ndustrial and, b... Standard [illegible]

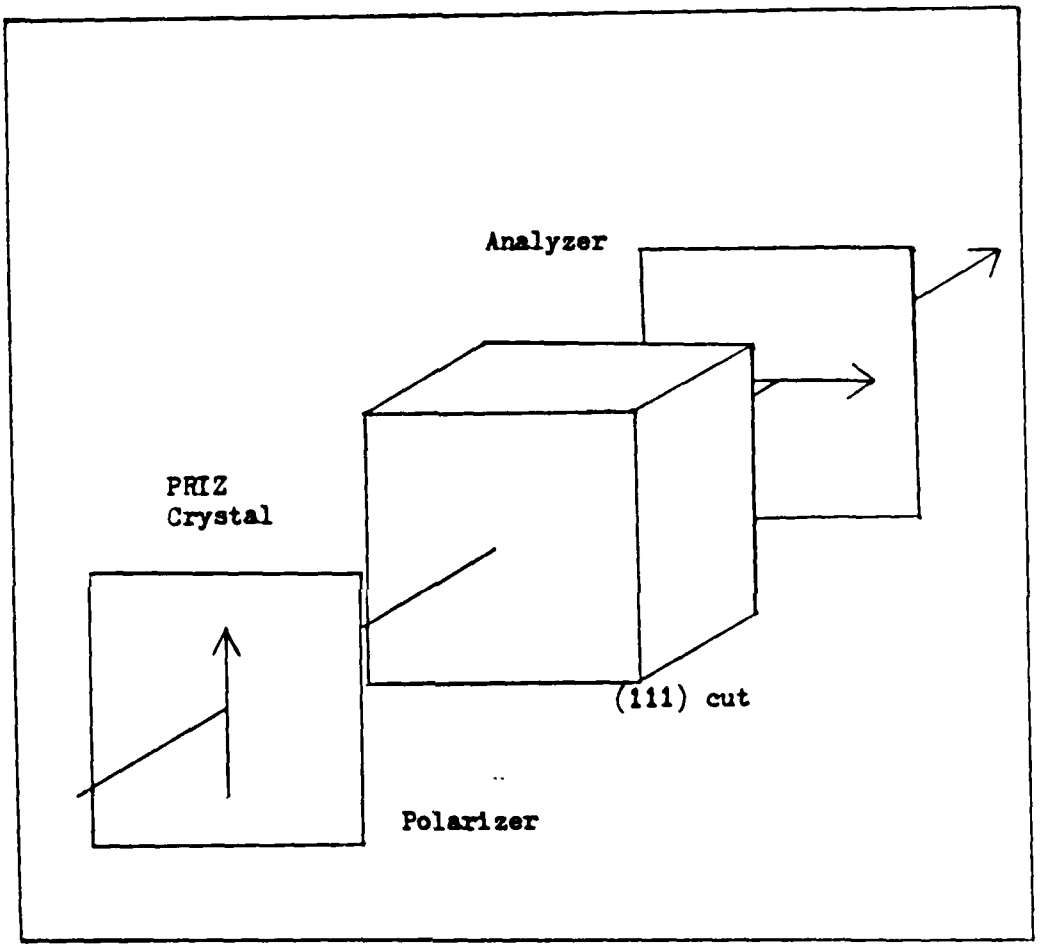

Figure 1.2. Complete PRIZ with polarizers for readout

sent through the device to interrogate the optical changes induced by the charge distribution in the crystal. The charge distribution is a map of the write beam which in a full application of the device would result from some kind of image. The read beam is sent through the device, parallel to the write beam. It is of a longer wavelength than the write beam. By having the read beam at a longer wavelength, the absorption coefficient is generally lower (17:12), as is the quantum efficiency (17:12). This reduces the number of electrons photo-excited by the read beam. The internal charge distribution of the crystal and the resulting electric field serve to modulate the index of refraction via the linear electrooptic effect (14:646). Since the internal electric field of the crystal is spatially varying, the local polarization of the beam is also spatially varying. The analyzer then provides a corresponding intensity variation (14:646).

Now that we have established the origin, nature, and importance of the internal electric field we can follow the development of Tanguay (14:646) to see how the phase difference of the device with a (111) crystal orientation can be calculated. The phase difference, Γ, is expressed as (16:817).

$$\Gamma = \frac{2\pi}{\lambda} \sqrt{\frac{2}{3}} n'^3 r_{63} E_t' d_o \qquad (1.1)$$

where λ is the wavelength of the incident light, n' is the unperturbed index of refraction and d_o is the longitudinal dimension of the crystal. E_t', the integrated transverse component, is given by

$$E_t' = \int_0^{d_o} E_{trans}(x,y,z)\, dz \qquad (1.2)$$

where E_{trans} is the electric field component perpendicular to the z axis.

The device can now be treated with standard electrooptic formalism, provided the phase difference is known. The quantity presenting the most difficulty in determining the phase difference is the longitudinally integrated transverse electric field. The balance of this paper will be devoted to finding a solution in some cases for this integral. The longitudinal field and the longitudinal charge density can be used to determine the transverse field.

Sequence of Presentation

Chapter II introduces the continuity and charge transport equations used to model the PRIZ device. The boundary conditions affecting the mathematical solution of the basic equations are discussed, and related to the

physical structure of the device. Existing analytic solutions are then presented.

The method of solution used in the computer model is presented in Chapter III. The numerical techniques used in the solution are reviewed, and the results of the model are presented. Where applicable, the solutions generated by the model are compared to predictions taken from the analytic solutions developed in Chapter II. The model is also extended into realms into which the analytic solutions are inapplicable.

In order to qualitatively evaluate PRIZ operation, including the transverse field, a simple example of an illuminated spot is treated in Chapter IV. The potential distribution through out the crystal is calculated and used to solve for the transverse fields, which are then integrated to give a solution for E_t'. Previous experimental observations are explained using this model.

Chapter V summarizes the results and includes recommendations for further theoretical and experimental efforts.

Chapter II

In order to investigate the temporal evolution of the fields within the PRIZ, the excitation process and subsequent charge transport and trapping are analyzed. A qualitative discussion of the mechanisms involved is presented, followed by an analysis of the basic equations of generation and transport. The relation of the type of PRIZ to the specifications of boundary conditions on the solutions is then examined. Finally, analytic solutions in several limiting cases are presented.

Qualitative Discussion

Before examining the basic equations governing PRIZ operation and identifying the operating regimes, it is helpful to discuss the PRIZ from a qualitative standpoint. The PRIZ operates by using an incident light beam to photo-excite electrons into the conduction band. Figure 2.1 is a diagram of the band structure. The primary source of electrons is the Si vacancy at 2.6 eV. The luminescence centers at 1.3 and 2.25 eV can also contribute electrons to the conduction band, if they are occupied. The excitation rate out of these levels is proportional to the power of the incident light. The absorption of the incident light in the bulk of the sample results in the excitation rate displaying an exponential decay consistent with Beer's law. Electrons

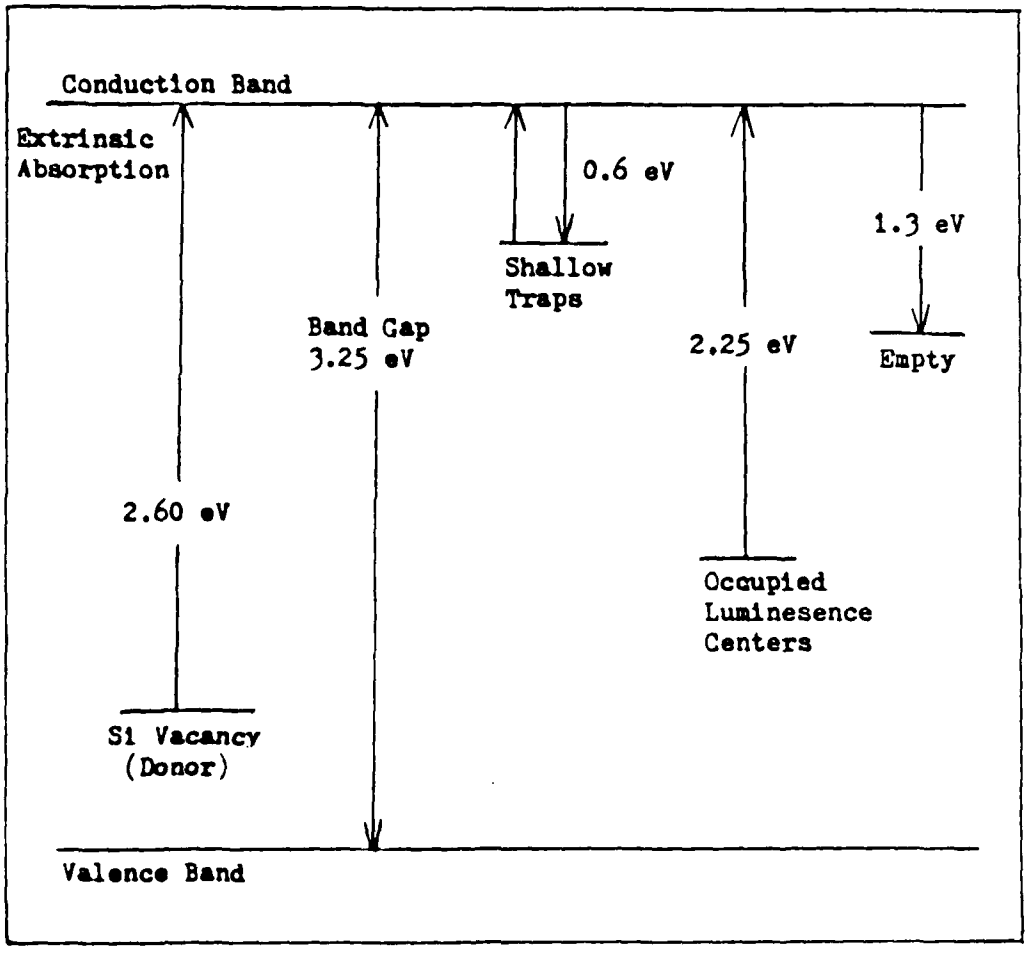

Figure 2.1. Energy Band Diagram of Bismuth Silicon Dioxide at Room Temperature (15:3684)

excited out of these levels leave behind a positively charged donor site.

Once in the conduction band, the electrons can then decay back into any one of the levels that has a hole available for recombination. The probability of the electron falling into the level is determined by the density of available sites to decay in, and the depth of the level in the band gap. Electrons which decay into the shallow traps can be reexcited with relative ease into the conduction band. The level at 1.3 eV is called a deep trap, due to the fact that electrons cannot be thermally excited out of this level, and the write light under consideration (400 to 500 nm.) does not have the appropriate energy to excite these levels to the conduction band. Thus conduction band electrons recombining to this level result in trapped, negatively charged centers.

The externally applied electric field causes transport of the electrons injected into the conduction band. For the standard bias conditions, the electrons drift away from the illuminated electrode and the holes drift toward it. Due to the relative immobility of the holes for the times under consideration, they will be treated as fixed throughout this study. Since the holes are immobile, and the electrons are moving away from the illuminated electrode, a region of positive space charge is formed just beyond the surface of the illuminated electrode. The shallow traps at 0.3 eV and

0.6 eV (10:878) can trap the electrons. Subsequent thermal excitation leads to a reintroduction of the electrons into the conduction band. The net effect is an apparent reduction in the mobility of the electrons in the conduction band. In contrast, since the electrons are trapped relatively permanently by the 1.3 eV level, a region of negative charge can form beyond the positive charge region. This process of generation, transport and subsequent trapping leads to charge separation. Between these two regions exists an interface where the charge density is neutral. The location of the interface is dependent on the ratio of the electron drift length and the absorption length.

When the total number of electrons excited into the conduction band is small, the charge densities created in the crystal do not generate a large enough self field to materially effect the applied field. This is referred to as the linear regime. The total longitudinal electric field in this regime can be approximated by the applied electric field. The linear regime is characterized by a stationary interface.

As the total number of electrons excited into the conduction band increases, the self field generated by the charge separation becomes significant compared to the applied field. The total charge shielding the applied field is greatest at the interface, thus the self field is largest at that point. Since the self field is oriented in

the opposite direction of the applied field, the magnitude of the total field is a minimum at the interface point. This is referred to as the "bottleneck". The velocity of the electrons in the conduction band is the product of their mobility and the local value of the electric field. Since at the bottleneck the field obtains its minimum value, the electron velocity is also at its minimum. This velocity reduction results in an enhanced trapping in the vicinity of the bottleneck, and a resultant migration of the interface point toward the illuminated electrode. Thus in the nonlinear regime, the interface moves toward the illuminated face of the crystal.

Basic Equations

The continuity equation yields the temporal variations of the local charge density within the crystal (5:82). The relevant equations for the densities of interest are:

$$e\frac{\partial}{\partial t}(n + n_- - n_+) = \nabla \cdot j \qquad (2.1)$$

$$\frac{\partial n_+}{\partial t} = gF(E) - \frac{nn_+}{\phi_d} \qquad (2.2)$$

$$\frac{\partial n_-}{\partial t} = \frac{n(n_t - n_-)}{\phi_t} - \frac{n_-}{\tau_{th}} \qquad (2.3)$$

The convective transport is described by the current density equation.

$$j = e\mu(nE_o - n\nabla\varphi + (kT/e)\nabla n) \qquad (2.4)$$

where

e = the modulus of the electron charge

$gF(R)$ = rate of electron excitation into the conduction band

R = the position vector

n_+ = density of positively charged donor sites

n_- = density of trapped electrons

n = density of electrons in the conduction band

n_t = density of traps

j = current density

φ_t = recombination time at deep traps

φ_d = recombination time at donor sites

τ_{th} = thermal ionization time of shallow traps

φ = potential due to internal charge distribution

E_o = externally applied electric field

μ = electron mobility

In order to simplify this system of equations, we will initially eliminate all nonlinear terms. Further, we will assume that the rate of excitation is transversely uniform, thus allowing $gF(R)$ to be expressed as simply $g \exp(-\alpha z)$, with α being the absorption coefficient. The thermal

diffusion of charge in the current expression, equation 2.4, will be ignored as this is small compared to the motion induced by the electric fields. Thermal excitation out of traps will be ignored. The thermal excitation is small compared to the photoexcitation. The total electric field will be expressed by

$$\mathbf{E} = \mathbf{E}_o - \nabla\varphi \tag{2.5}$$

Within these approximations, the system of equations is:

$$\frac{\partial}{\partial t}(n + n_- - n_+) = \mu\nabla\cdot(n\mathbf{E}) \tag{2.6}$$

$$\frac{\partial n_+}{\partial t} = g\ \exp(-\alpha z) \tag{2.7}$$

$$\frac{\partial n_-}{\partial t} = \frac{n}{\tau_t} \tag{2.8}$$

where τ_t, the lifetime of an electron in the conduction band, is given by φ_t/n_t. Equation 2.6 relates the time rate of change of the total charge density of the sample to the divergence of the current. Equation 2.7 states that the time rate of change of the positively charged donor site density is simply the excitation rate, g(z). While in

equation 2.8, the time rate of change of the negatively charged trap site density is governed by the decay rate of electrons from the conduction band.

We are initially interested in only the longitudinal electric field in equation 2.6 because we must have the complete solution for the longitudinal field and space charge density before examining the transverse fields. Substituting the equations 2.7 and 2.8 into equation 2.6 yields the time rate of change of the conduction band density.

$$\frac{\partial n}{\partial t} = g(z) - \frac{n}{\tau_t} + \mu\frac{\partial}{\partial z}(En) \qquad (2.9)$$

where E is the z-component of the vector **E** and z is the direction parallel to the light beam propagation. With equations 2.7-9 we have a complete description of our simplified system.

Boundary Conditions

Two different PRIZ devices have been constructed or described previously in the literature (12:1). The first is the "standard" PRIZ, Figure 1.1b. Here the crystal is separated from each electrode by a dielectric layer. Thus the crystal remains charge neutral since no charge can traverse the dielectric barriers. The boundary conditions

on the currents at either face of the crystal are

$$j(0,t) = 0 \tag{2.10}$$

$$j(d_o,t) = 0 \tag{2.11}$$

where d_o is the length of the crystal in the z direction.

The second PRIZ device is the "conducting" PRIZ, Figure 1.1a. The insulating dielectric layer is omitted from this device. Without the insulating dielectric, the boundary conditions are described by

$$j(0,t) = \text{injection current} \tag{2.12}$$

$$j(d_o,t) = \mu e\Big[\, E(d_o,t)\; n(d_o,t)\Big] \tag{2.13}$$

where the injection current will be dependent on the electric field at the illuminated face of the crystal versus the barrier potential. In most cases the injection current represented by equation 2.12 is very small compared to the current represented by equation 2.13, so $j(0,t) = 0$. The bulk of this paper will deal with the "conducting" version of the PRIZ.

Operating Regimes

As discussed previously in the qualitative discussion, there are two operating regimes of the PRIZ which depend on the total charge generated by the write beam. The excitation rate, g(z), can be related to the intensity, I of the write beam by (10:879)

$$g(z) = \frac{I(z)\alpha f_Q}{h\nu} \tag{2.14}$$

where f_Q is the experimentally obtained quantum efficiency at any given wavelength and $h\nu$ is the photon energy. A characteristic time, t_o, divides the linear and nonlinear regimes of operation, where (9:1349):

$$t_o = \frac{n_o d_o}{g(0)\mu|E_o|\tau_t} \tag{2.15}$$

with

$$n_o = \frac{\epsilon'}{e\mu\tau_t} \tag{2.16}$$

where ϵ' is the total dielectric constant of the material. Physically, the time t_o is the length of time that must elapse before the self field is the same order of magnitude

as the imposed field.

Linear Regime

Regardless of the initial write beam intensity, the PRIZ device always starts in the linear regime. From equation 2.15, the excitation rate, g(0), will determine the length of time that the device will spend in the linear regime. The linear regime is characterized by an electric field which can be approximated everywhere by E_o and a stationary interface point. Approximating E by E_o means that E is no longer dependent on the conduction band density, n, so equation 2.9 is a linear equation, thus this regime is referred to as linear.

Since the longitudinal electric field can be approximated everywhere by E_o, no bottleneck arises. If we define the total charge number density as

$$\rho = n_+ - n - n_- \tag{2.17}$$

and replace E by E_o, then the charge number density can be represented analytically by (8:687)

$$\rho = \frac{gt}{\left(1 - \gamma \right)} \left[\exp\left[\frac{-z}{\mu |E_o| \tau_t} \right] - \gamma \exp\left[-\alpha z \right] \right] \tag{2.18}$$

where $\gamma = \alpha\mu|E_o|\tau_t$. Since by definition, the charge density is zero at the interface, setting equation 2.18 to zero and solving for z gives the location, z_o, of the interface. (6:1688)

$$z_o = \frac{\ell \ln(\gamma)}{(\gamma - 1)} \tag{2.19}$$

where ℓ is the drift length, $\mu|E_o|\tau_t$. The interface z_o is stationary throughout the linear time regime.

We can now determine the electric field arising from this charge distribution. In a one-dimensional approximation, the normalized longitudinal field can be calculated in terms of the normalized charge density as:

$$\frac{\partial \delta}{\partial z} = - \frac{\rho(z)}{n_o} \tag{2.20}$$

where $\delta = |E|/|E_o|$. Integration yields

$$\delta = \frac{g(0)t}{n_o(1-\gamma)} \exp\left[\frac{-z}{\ell}\right] - \frac{g(0)t}{n_o(1-\gamma)} \exp\left[-\alpha z\right] + C_1 \tag{2.21}$$

where C_1 is the constant of integration. For a given potential constant across the PRIZ, the value of C_1 is established. This allows us to express the total

longitudinal field as

$$|E| = |E_o| + \frac{|E_o| g(0) t}{n_o(1-\gamma)} \left\{ \exp\left[-z/\ell\right] - \exp\left[-\alpha z\right] \right\} +$$

$$\frac{|E_o| g(0) t}{n_o(1-\gamma)} \left\{ \frac{\ell}{d_o}\left[\exp\left[-d_o/\ell\right] - 1\right] + \frac{1}{\alpha d_o}\left[1 - \exp\left[-\alpha d_o\right]\right] \right\} \quad (2.22)$$

where d_o is the length of the crystal. This represents the complete solution for the electric field in the linear regime.

Linear Regime, Electric Field Dependence on the Absorption Coefficient

The form of the electric field, equation 2.22, can be simplified by considering two cases: when the absorption coefficient is small, and when the absorption coefficient is large. In the case of a small absorption coefficient which corresponds to uniform illumination and $g(z) = g(0)$, Bryskin has approximated the charge distribution given by equation 2.18 (7:31)

$$\rho = gt \, \Theta\left[\frac{z_o}{\ell} - \frac{z}{\ell} \right] \quad (2.23)$$

where $\Theta(x)$ is the Heaviside function. Using this approximation for ρ and following the same procedures for the complete solution for ρ , the electric field is given by

$$|E| = \begin{cases} \dfrac{gt(z_o - z)}{n_o \mu \tau_t} + |E_o| - \dfrac{|E_o| g t z_o^2}{2 d_o n_o \ell} & z \le z_o \\ |E_o| - \dfrac{|E_o| g t z_o^2}{2 d_o n_o \ell} & z \ge z_o \end{cases} \qquad (2.24)$$

where z_o is as defined by equation 2.19. Examining equation 2.24, we can see that the field at the illuminated face of the crystal grows linearly with time, and beyond the interface, z_o, the field is independent of position. This holds true only for the case where α is small.

Now consider the case where the device is still operating in the linear regime but the absorption coefficient is large. There is no equivalent simplifying approximation to make for the space charge density as there was when the absorption coefficient was small. We instead will examine equation 2.21 and see how we can simplify that expression. In cases where α is large, we can discard the term $\exp(-\alpha d_o)$. Therefore we have the following approximation for the field

$$|E| = |E_o| + |E_o|B\left\{\exp(-z/\ell) - \exp(-\alpha z)\right\}$$

$$+ |E_o|B\left\{\frac{\ell}{d_o}\left[\exp(-d_o/\ell) - 1\right] + \frac{1}{\alpha d_o}\right\} \qquad (2.25)$$

with

$$B = \frac{g(0)t}{n_o(1-\gamma)} \qquad (2.26)$$

Thus we have an approximation to what the field will look like in the case of strong absorption.

Nonlinear Regime

In the case where the total charge created is large enough to produce a self field on the order of the applied field, equation 2.9 becomes non-linear in the charged particle density. The electric field increases in the vicinity of the illuminated electrode and obtains a minimum value, less than E_o, at the interface location, z_o. This minimum leads to a bottleneck in the flow of electrons. At the bottleneck the electron velocity is severely restricted and the relative probability of being trapped in this region is in turn raised. This increased trapping produces a

migration of the interface toward the illuminated electrode.

The rate of accumulation of the integrated longitudinal charge in the crystal, Q, is the prime driver behind the change in the electric field value. Q is actually a surface charge density generated by the charge distribution function, ρ. An analytic description due to Bryskin starts by defining how the total charge surface changes with time (7:30)

$$\frac{dQ}{dt} = j(0,t) - j(d_o,t) \qquad (2.27)$$

where $j(0,t)$ is the injection current and $j(d_o,t)$ is the current leaving through the dark face. From equation 2.4 the current j can be written as

$$j = e\mu nE \qquad (2.28)$$

Bryskin then assumes that we are again operating where the absorption coefficient, α, is small. Using the approximation in equation 2.23 to find the surface charge density, Q, yields

$$Q = gtz_o \qquad (2.29)$$

If we assume the injection current vanishes, all we need

worry about is the current traversing the dark face. We can write the field in the region beyond the interface using equation 2.24. Substituting this field into equation 2.28 and then substituting equation 2.28 and 2.29 into 2.27 yields

$$\frac{d}{dt}\left[gtz_o\right] = \mu n(d_o,t)|E_o|\left[1 - \frac{gtz_o^2}{2d_o n_o \ell}\right] \qquad (2.30)$$

We now have the increase in the surface charge density in the crystal defined by the current leaving the crystal in terms of the electric field approximation in the case of α small.

Bryskin next finds an expression for the electron conduction band density at the dark face. Approximating equation 2.17 by

$$\rho = gt - n_- - n \qquad (2.31)$$

and using the fact that in our approximation $\rho = 0$ beyond z_o, allows us to rewrite equation 2.8 as

$$\frac{\partial n}{\partial t} + \frac{n}{\tau_t} = g \qquad z \geq z_o \qquad (2.32)$$

using the initial conditions $n(z,0) = 0$, the solution to

equation 2.32 is

$$n = g\tau_t\left[1 - \exp\left[\frac{-t}{\tau_t}\right]\right] \tag{2.33}$$

In the nonlinear regime $t >> \tau_t$, so we will neglect the exponential term in equation 2.33. Now we can write equation 2.30 as

$$\frac{d}{dt}\left[tz_o\right] = \ell\left[1 - \frac{gtz_o^2}{2d_o n_o \ell}\right] \tag{2.34}$$

At large times the solution can be written (7:32)

$$z_o = \left[\frac{2V\epsilon'}{eg(0)t}\right]^{1/2} \tag{2.35}$$

Solving equation 2.24 for the illuminated face of the crystal and approximating for times $t >> t_o$ yields an expression for the field at the illuminated face of the crystal (7:32)

$$| E(0,t) | = \left[\frac{2eg(0)tV}{\epsilon'}\right]^{1/2} \qquad (2.36)$$

where V is the applied potential, and ϵ' is the dielectric constant for the crystal. For cases when α is large, this analysis is inappropriate and numerical methods must be used.

Astratov Solution

Now we have identified a need for an iterative numerical solution for certain cases of operation of the PRIZ, notably the transition region between the linear regime and the nonlinear regime and the nonlinear regime for cases where the absorption coefficient is large. Astratov has presented a numerical solution of the conduction band density, longitudinal electric field and space charge density assuming a quasi-steady state (3:1586):

$$\frac{\partial n}{\partial t} \approx 0 \qquad (2.37)$$

Unlike the previous analysis of Bryskin, he assumes that the source term g(z) results solely from thermal excitation of electrons from previously uniformly populated shallow traps. The excitation term, g(z,t), decays with time as the population relaxes thermally with relaxation time, τ_{th}.

Thus (3:1585)

$$g(t) = g(0)\exp\left[- \frac{t}{\tau_{th}} \right] \qquad (2.38)$$

With the assumption made in equation 2.37 it becomes possible to solve equation 2.9 analytically with the boundary conditions specified by equations 2.12 and 2.13. The solution becomes discrete as the partial derivative with respect to z is approximated by Δz. Equation 2.9 is set equal to zero and solved by employing the integrating factor approach (4:350). Astratov obtains an expression for n(z) at fixed points in the crystal, the points designated by the integer i

$$n(z_i) = \frac{E(z_{i-1})}{E(z_i)} n(z_{i-1}) \exp\left[- \frac{\Delta z}{\mu |E(z_i)| \tau_t} \right] +$$

$$g(t)\tau_t \left[1 - \exp\left[- \frac{\Delta z}{\mu |E(z_i)| \tau_t} \right] \right] \qquad (2.39)$$

where $E(z_i)$ is the field at the specified point and Δz is the distance in between specified points. The total charge number density is found by adding the existing density at time t to the conduction band density at $t+\Delta t$ and the fixed

charge at t+Δt

$$\Delta\rho_f(z_i) = \left[g(t) - \frac{n(z_i)}{\tau_t}\right]\Delta t \qquad (2.40)$$

Therefore, the total charge number density can be found by the following expression

$$\rho(z_i,t+\Delta t) = \rho(z_i,t) + \Delta\rho_f(z_i) - n(z_i) \qquad (2.41)$$

The electric field at any point i is calculated by taking the charge density at all points i, assuming the charge to be distributed in an infinite plane, and summing each planes contribution to the electric field at the point i. Once the new electric field is found, the g(t) term is advanced by Δt and the solution can proceed iteratively through time.

The Astratov solution is flexible enough to accept other types of time dependent excitation merely by rewriting g(t) appropriately. It is possible to extend Astratovs' basic solution to a more general form which treats absorption. In order to treat absorption, it is necessary to start again with the basic set of equations and solve using the new form of g(z). Writing the excitation rate to include absorption, $g(z) = g(0)\exp(-\alpha z)$, the solution to $n(z_i)$ is found to be

$$n(z_i) = \frac{E(z_{i-1})}{E(z_i)} n(z_{i-1}) \exp\left[- \frac{\Delta z}{\mu |E(z_i)| \tau_t} \right] +$$

$$\frac{g(0,t)\tau_t}{\mu E(z_i)\tau_t \alpha + 1} \left\{ \exp\left[-z_i \alpha\right] - \exp\left[- \frac{\Delta z}{\mu |E(z_i)| \tau_t} - z_{i-1} \alpha \right] \right\} \quad (2.42)$$

The solution to the modified Astratov proceeds as outlined previously.

The Astratov solution is not valid for times in which the conduction band density is rapidly changing. In addition, the method provides no guidance for numerical stability, the solution can be overdriven if the time step is too large, and no provision exists in either the Astratov solution or the modified Astratov solution to correct a time step that is too large. The Astratov solution is also limited to the simplified system, equations 2.6-8, if an additional term is to be examined, the system must be resolved, if indeed, that is even possible.

Chapter III

The previous chapter identified two operating regimes of the PRIZ. This chapter presents a numerical solution of the system of equations 2.7-9 which is applicable in either operating regime. The method used to solve the system of equations will be presented, followed by comparisons of the numerical solutions with analytic results. Normal PRIZ operating conditions, however, do not satisfy many of the assumptions on which these analytic solutions were based. Therefore, the numerical model will be used to examine solutions under these conditions.

Numerical Model Development

From the system 2.7-9, we can develop a system of two equations which can be used to find the total charge in the sample. The first equation of interest is equation 2.9.

$$\frac{\partial n}{\partial t} = g(z) - \frac{n}{\tau_t} + \mu \frac{\partial}{\partial z}\left(En\right) \qquad (3.1)$$

By defining a new term, $\rho_f = n_+ - n_-$, we can find the time rate of change of ρ_f by subtracting equation 2.7 from equation 2.8. This yields

$$\frac{\partial \rho_f}{\partial t} = g(z) - \frac{n}{\tau_t} \qquad (3.2)$$

Equation 3.1 contains differentials of two different variables, z and t. The derivative with respect to z can be approximated as a difference to give the following

$$\frac{\partial n\left[z_i,t\right]}{\partial t} = g\left[z_i\right] - \frac{n\left[z_i,t\right]}{\tau_t} + \frac{\mu}{\Delta z}\left\{ n\left[z_i,t\right]\ E\left[z_i,t\right] - n\left[z_{i-1},t\right]\ E\left[z_{i-1},t\right]\right\} \qquad (3.3)$$

where Δz is the distance between the discrete bins designated by the subscript i. Referring back to Figure 1.1, we have divided the crystal longitudinally into m slices, where the index numbered 0 is at the write beam side and the index numbered m is at the opposite side. The first term to the right of the equals sign in equation 3.3 is the local rate of excitation into the conduction band. The second term is the rate of electron decay out of the conduction band due to trapping. The last term in the brackets approximates the divergence of the conduction band electron flux. We thus have a system of m coupled, first-order, nonlinear equations which describe the density of conduction band electrons in the crystal. We rewrite

equation 3.2 as

$$\frac{\partial \rho_f\left[z_i,t\right]}{\partial t} = g\left[z_i\right] - \frac{n\left[z_i,t\right]}{\tau_t} \qquad (3.4)$$

Here, $g(z_i)$ represents the rate of production of fixed positive charge sites at the position z_i. The second term represents the formation rate of fixed negative charge sites. The total net charge at any given time can be found by subtracting the conduction band density from the net fixed charge.

$$\rho\left[z_i,t\right] = \rho_f\left[z_i,t\right] - n\left[z_i,t\right] \qquad (3.5)$$

Once the charge density at every point is known, the electric field at every point can be calculated. This is most easily done in a one dimensional approach by assuming the charge density at each point is distributed in an infinite plane. The value of the electric field at any point z_i, is found by

$$E\left[z_i,t\right] = -E_o + \sum_{k=1}^{i} \frac{\sigma_k}{2\epsilon\epsilon_o} - \sum_{k=i+1}^{m} \frac{\sigma_k}{2\epsilon\epsilon_o} \qquad (3.6)$$

where $\sigma_k = \rho(z_k)A_r$, the area charge density at any discrete point k, A_r is the area of the PRIZ crystal, ϵ is the dimensionless dielectric constant of the crystal and ϵ_o is the dielectric constant of free space. The charge density and electric field are calculated self-consistently at each time, t.

The IMSL Fortran subroutine, DGEAR (11:8), was chosen to solve the equations 3.3 and 3.4 as a system of first order differential equations. DGEAR was appropriate because the subroutine uses backward differentiation for stiff equations. Also, DGEAR is designed to handle an initial condition problem, and the initial conditions of the PRIZ are very easy to write,

$$n\left[z_i,0\right] = 0 \tag{3.7}$$

$$\rho_f\left[z_i,0\right] = 0 \tag{3.8}$$

The spatial boundary conditions of the conducting PRIZ were specified by modifying equation 3.3 at the points where i = 1 and i = m. The boundary condition at the illuminated face was specified by eliminating the flux into the first bin, equation 2.12. The boundary condition at the dark face

was specified by allowing the free escape of conduction band electrons into a dummy discrete point, m+1.

Conducting PRIZ Device

The device modeled in the remainder of the chapter is a PRIZ constructed of a (111) cut BSO crystal. The dielectric constant, ϵ, is 56.0. The mobility of the electrons, μ, is 3.0×10^{-6} $m^2/(sec\text{-}V)$. The lifetime of the electrons in the conduction band, τ_t, is 3.0×10^{-5} sec. The crystal parameters listed above are taken from ref. 8. The 1cm · 1cm × 1mm crystal has a potential of 2000V applied across the 1mm dimension. It is assumed that this potential difference is maintained throughout the period of operation. This yields a drift distance, $\ell = 1.8 \times 10^{-2}$ cm. Three write beam wavelengths are used in order to examine the sensitivity to wavelength variations in the absorption coefficient. Weak absorption corresponds to, λ = 589 nm and $\alpha_1 = 0.6$ cm^{-1}; strong absorption, λ = 400 nm and $\alpha_3 = 90.0$ cm^{-1}. Intermediate comparisons at, λ = 434 nm and $\alpha_2 = 45.0$ cm^{-1} are also included (17:13). The data presented assumes that the excitation rate at the illuminated face of the crystal, g(0), is constant for all cases. This results in the excitation of a larger number of charge carriers as the absorption coefficient becomes smaller. Conversions back to incident power can be made using equation 2.14.

Linear Regime, Comparisons with Complete Solutions

For the linear regime, where $t << t_o$, there exist analytic forms which can be used to predict both the space charge density, equation 2.18, and the longitudinal electric field, equation 2.22. For cases in which the absorption coefficient, α, is small, these equations simplified to charge density, equation 2.23, and electric field, equation 2.24, respectively. When the absorption coefficient is large, the electric field was shown to be approximated by equation 2.25. Comparisons of the numerical results with the analytic forms, and both sets of approximations will be presented in this section. In order to insure that the linear regime approximation is valid, $t = .01t_o$, for all comparisons.

The first comparison to consider is that of the numerical solution to the exact analytic forms which exist. Figures 3.1-3 compare the predictions of equation 2.18 to the results yielded by the numerical solution for small, medium and large absorption coefficients. The curves can be seen to exhibit excellent agreement, the point of greatest disparity is in the prediction of the point z_o. For α_1 the difference as a fraction of the total crystal length is 5.36%. For α_2, the difference is 1.57%. For α_3, the difference is 1.57%.

The surface charge number density of the PRIZ, Q, is the determining factor in the strength of the self electric

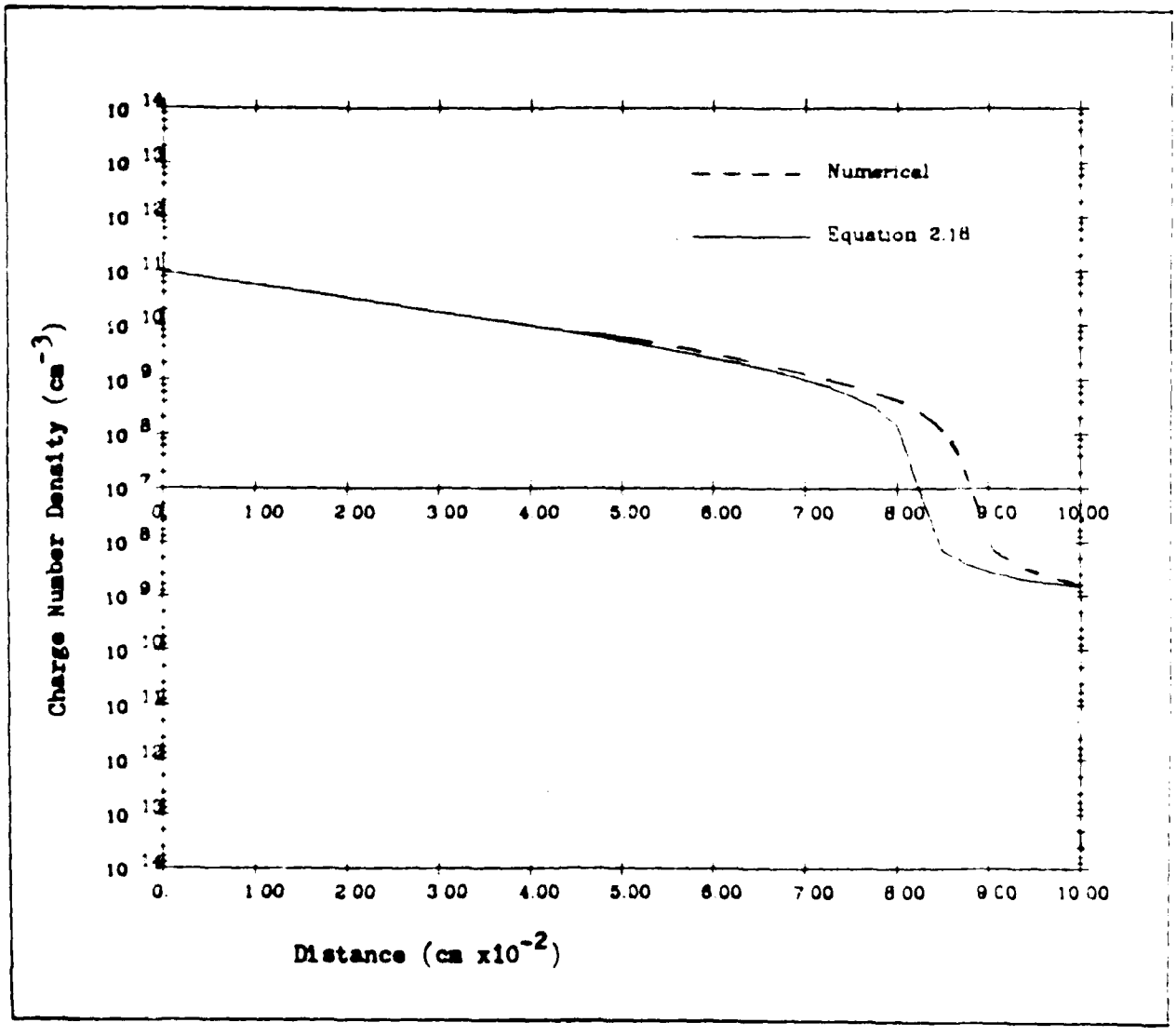

Figure 3.1. Linear Regime, Longitudinal Charge Number Density for small Absorption Coefficient, $\alpha = 0.6\ cm^{-1}$, $t = .01t_o$

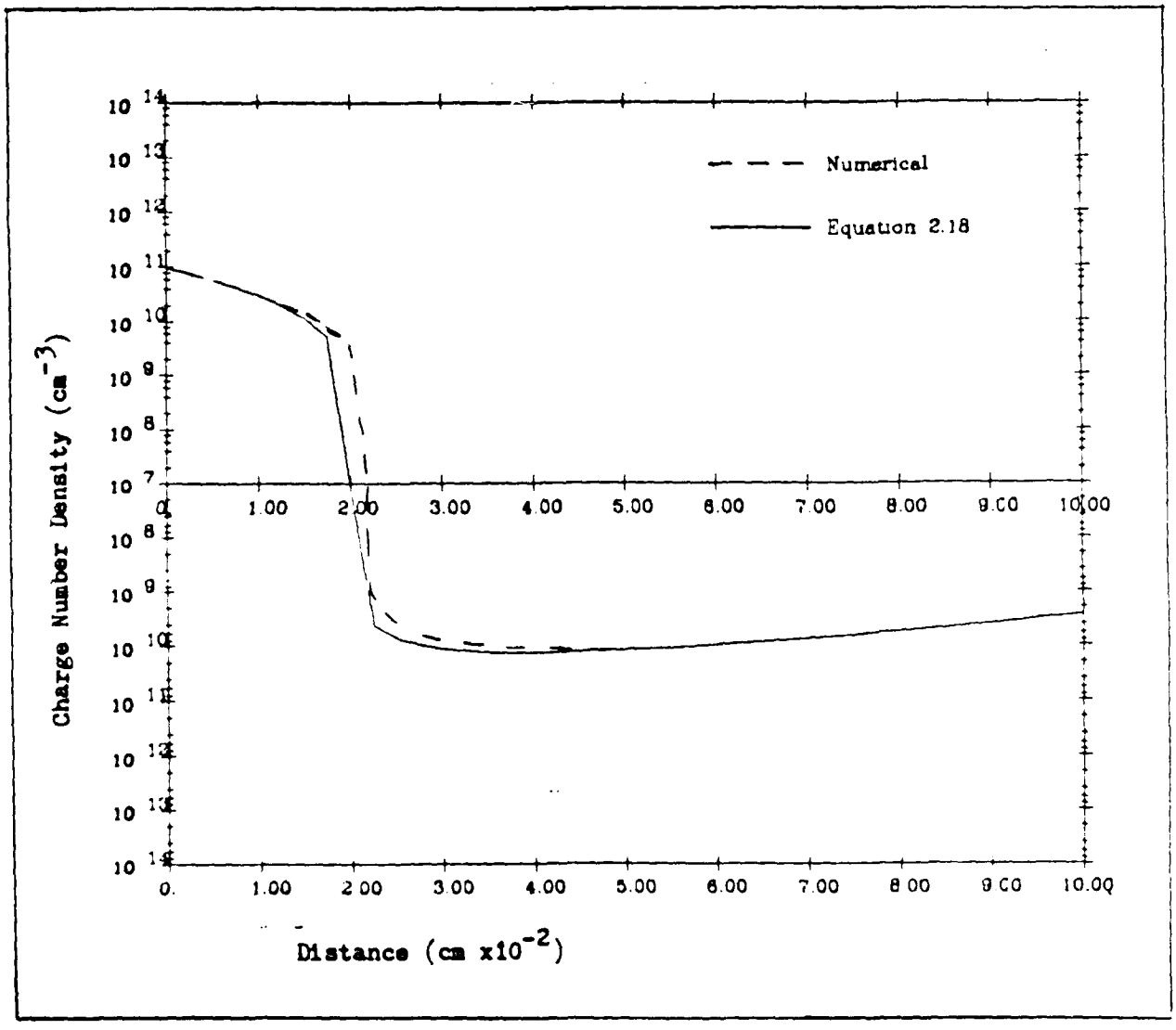

Figure 3.2. Linear Regime, Longitudinal Charge Number Density for medium Absorption Coefficient, $\alpha = 45\ cm^{-1}$, $t = .01t_o$

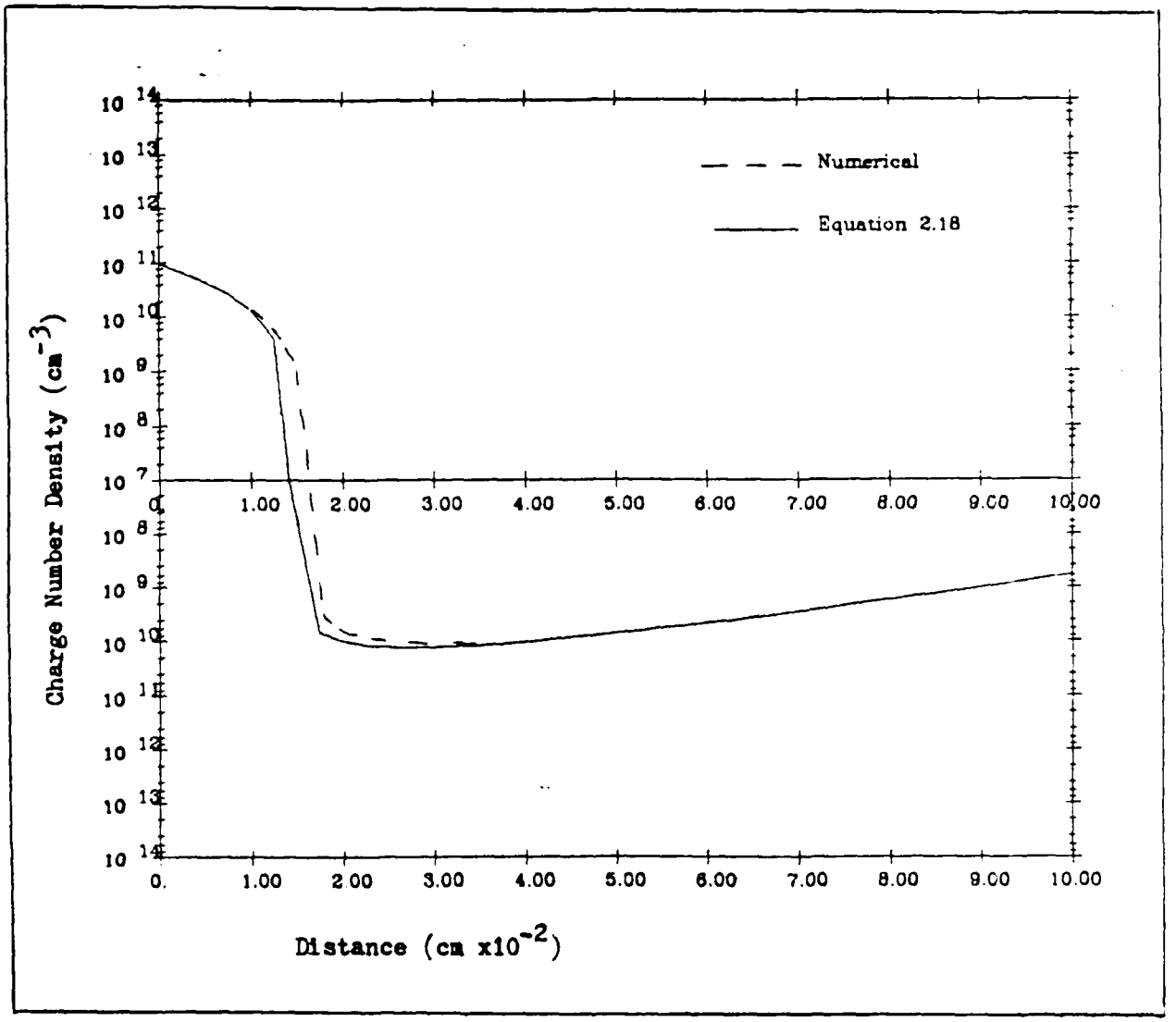

Figure 3.3. Linear Regime, Longitudinal Charge Number Density for large Absorption Coefficient, $\alpha = 90\ cm^{-1}$, $t = .01t_o$

field. To analytically calculate the surface charge number density, Q, we integrate equation 2.18, which yields

$$Q = \frac{g(0)t\ell}{1 - \gamma}\left[\exp\left[-\alpha d_o\right] - \exp\left[-d_o/\ell\right]\right] \qquad (3.9)$$

From the numerical solution, the surface charge number density can be numerically integrated using the trapezoid rule. For α_1, the difference between the analytic form and the numerical Q is 0.24%. The analytic value for Q is slightly larger than the numerical value for Q. For α_2, the difference is 2.91%, with the larger value being predicted by the numerical solution. For α_3, the difference is 8.3%. The numerical solution again predicts the larger value. These results agree quite well and are expected from the correlation of the charge density curves.

Now we will compare the predictions of the complete solution to the longitudinal electric field, equation 2.22, with the numerical solution. Equation 2.22 is derived using the analytic form of the charge density, equation 2.18. The total field E is not compared, rather, the self field generated by the internal charge distribution only will be plotted. The self field at the illuminated face of the crystal can be calculated directly from the total charge number density, Q. The greatest disparity in the solutions

occurs in calculating the self field at the illuminated face of the crystal. For α_1, the numerical solution is the larger of the two and the difference between them is 18.9%. For α_2, the numerical solution is again larger and the difference is 7.0%. For α_3, the numerical solution is larger and the difference is 17.9%.

The numerical solution is sensitive to the grid size chosen. In order to demonstrate this, the number of bins was increased to 2m, in the case where $\alpha = \alpha_1$. This resulted in a tenfold increase of computer time. The agreement between the values for Q is 0.15%. For the electric field at the illuminated face of the crystal the difference is 0.96%. Figure 3.4 displays the numerical solution for the electric field only, since the two solutions are essentially the same. Figure 3.5 and 3.6 show the comparison between the numerical forms and the form of equation 2.22. Both Figure 3.5 and 3.6 were calculated with m discrete points.

Figure 3.4 shows the result when the crystal contains an essentially positive charge distribution is present throughout the crystal. The charge distribution for this is shown in Figure 3.1. Figures 3.5 and 3.6 show the results for the crystal when there is a positive region and a negative region, these charge distributions are shown in Figures 3.2 and 3.3, respectively. The field actually forms a slight bottleneck and then increases again due to the

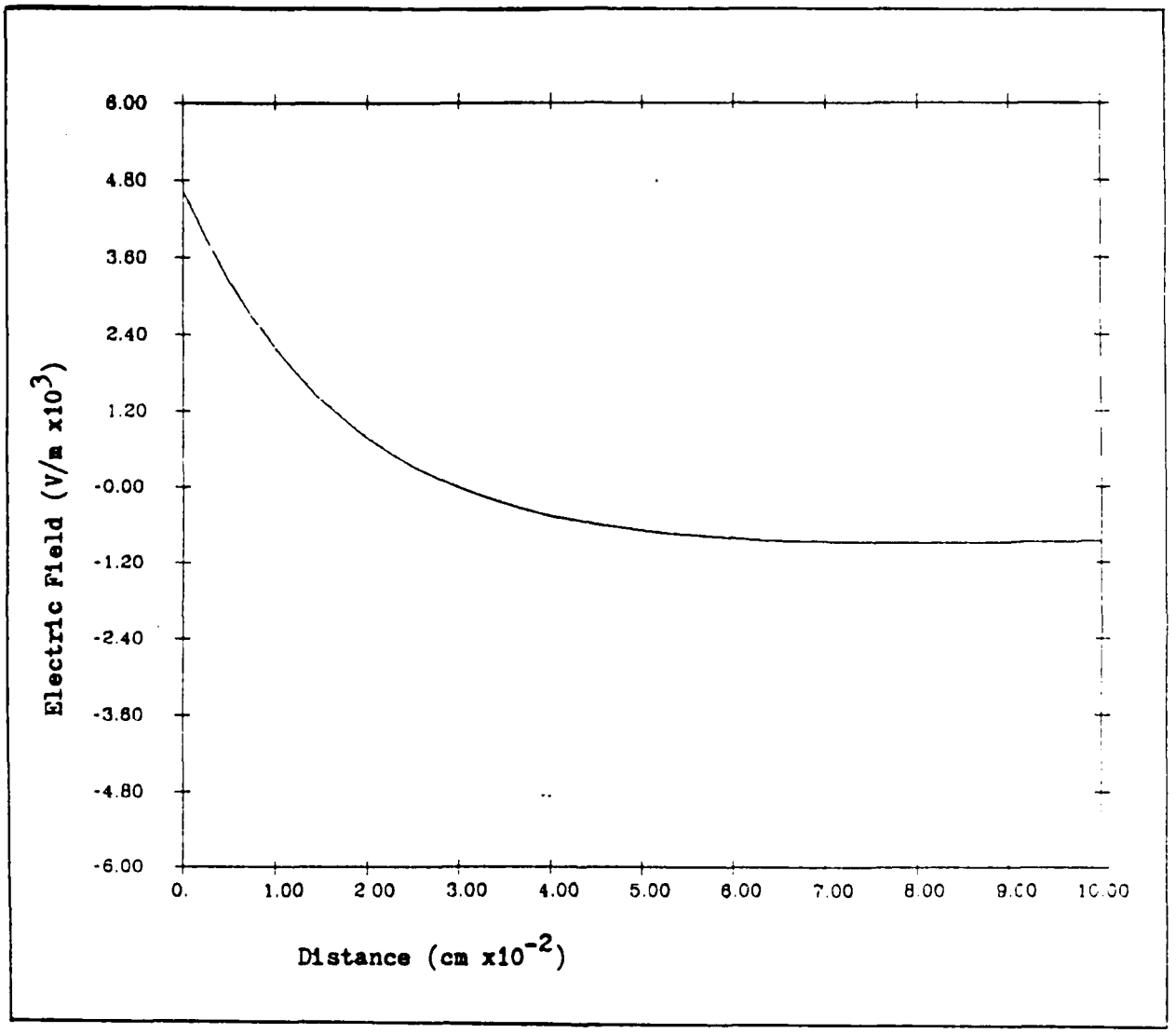

Figure 3.4. Linear Regime, Longitudinal Self Electric Field for $\alpha = 0.6\ cm^{-1}$, $t = .01t_o$

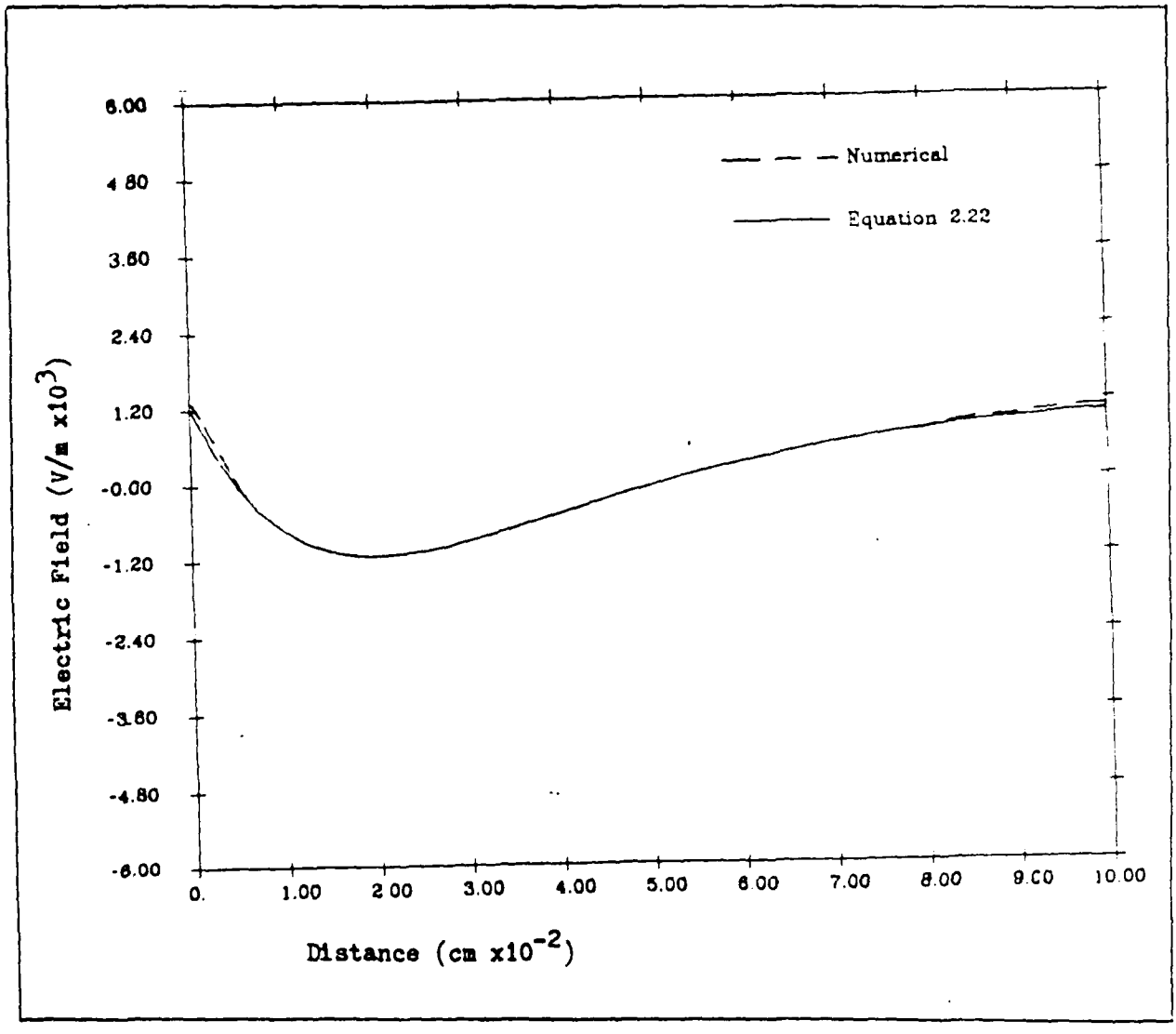

Figure 3.5. Linear Regime, Longitudinal Self Electric Field for $\alpha = 45\ cm^{-1}$, $t = .01t_o$

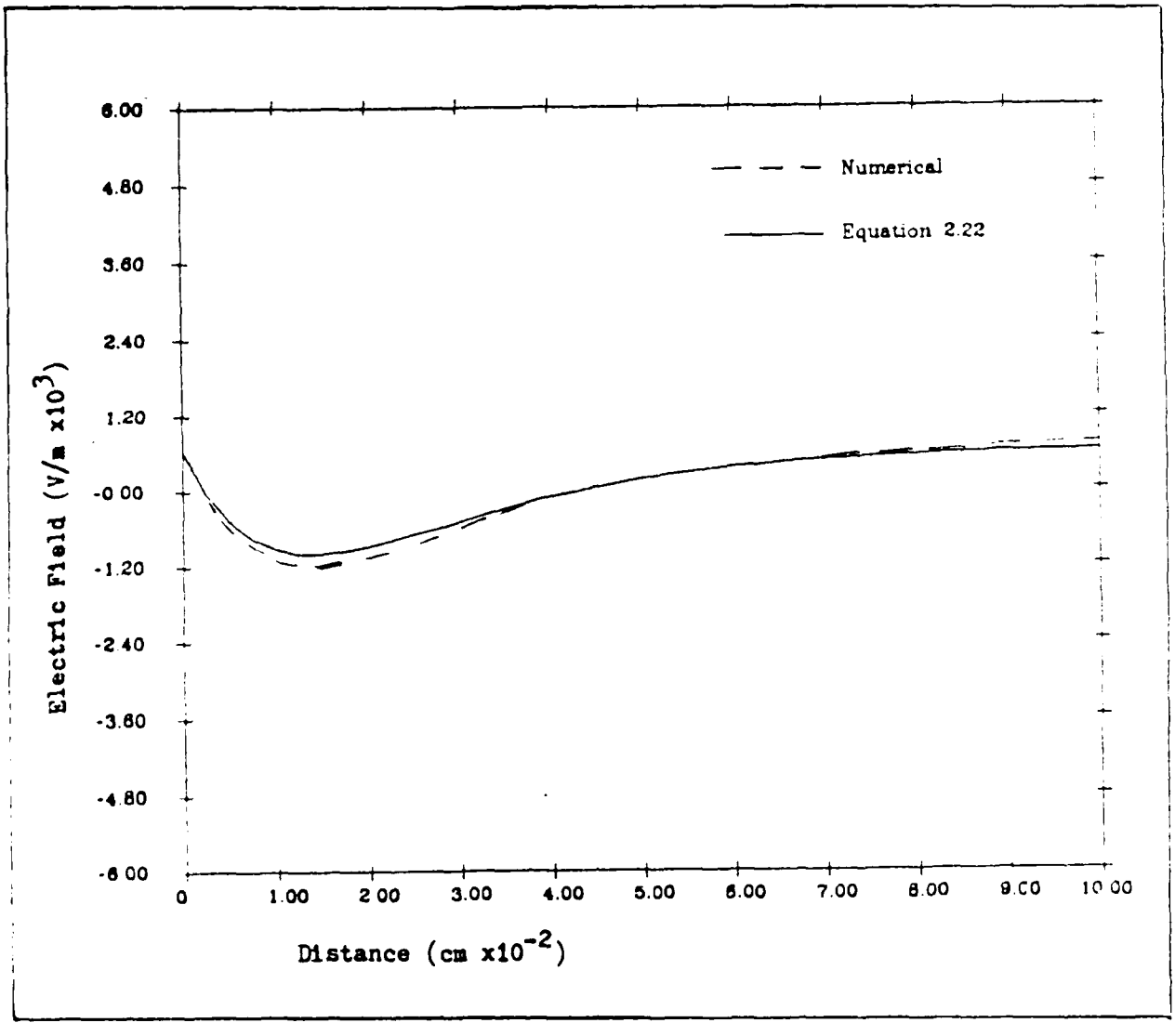

Figure 3.6. Linear Regime, Longitudinal Self Electric Field for $\alpha = 90\ cm^{-1}$, $t = .01t_o$

negative charge region.

The analytic forms that Bryskin derives for the linear regime work quite well when the time under consideration is well within the linear regime. The complete solution for the electric field, equation 2.22, derived in this study matches excellently with the numerical solution. The numerical solution produces acceptable results in a short amount of computer time. If computer time is not restricted, the results available to the numerical solution are excellent.

Linear Regime, Comparisons with Approximate Solutions

The analytic solutions developed in Chapter II were analyzed for their behavior in limiting cases of the absorption coefficient. These limiting cases were when α is small and when α is large. The numerical solution developed in this chapter will be compared to the limiting forms.

The numerical solution can be used to find the space charge density, $\rho(z)$, in the limiting case of α small. The approximation for $\rho(z)$ is given by equation 2.23. Using α_1 as the absorption coefficient that is small, Figure 3.7 shows the curves generated by both the numerical solution and the approximation. The form of these curves does not compare favorably, so the best way to check for the validity of the approximation is to compare the value of the total charge on the PRIZ, Q. Equation 2.23 can be seen to predict

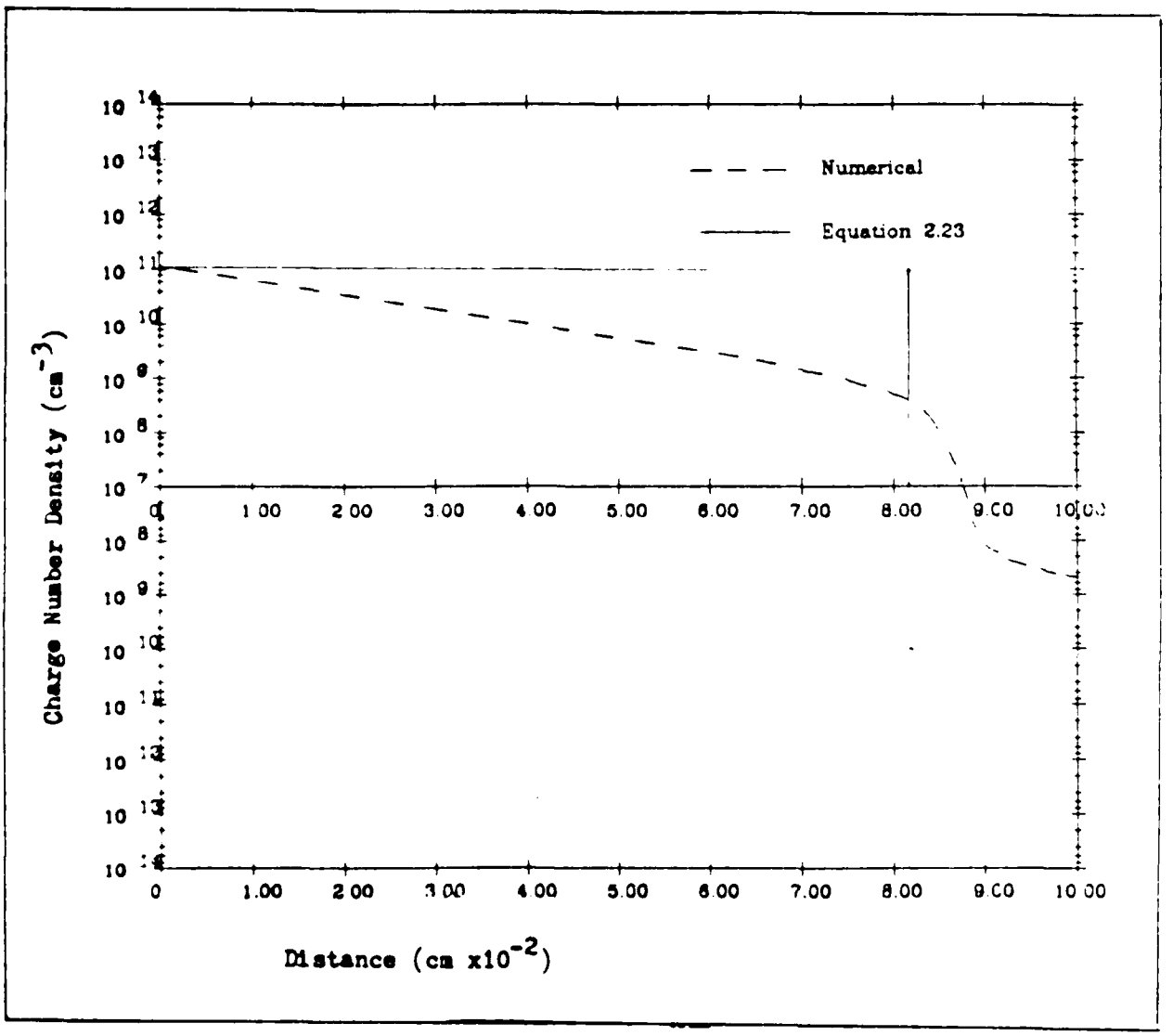

Figure 3.7. Linear Regime, Longitudinal Charge Number Density for $\alpha = 0.6\ cm^{-1}$, $t = .01t_o$

a larger value of Q than that of the numerical solution. The approximate value of Q is 4.8 times the value of Q yielded by the numerical solution. This does not agree nearly as well as the analytic expression given in equation 2.18 does.

Using the charge density approximation, equation 2.23, the electric field can be calculated. This expression is given in equation 2.24. A comparison of the two curves is shown in Figure 3.8. The value of the electric field at the illuminated face of the crystal is clearly larger for the approximation than that of the numerical solution. This is expected due to the fact that the approximation severely over predicted the total charge present in the crystal. The value of the approximate solution is 1.72 times the numerical solution.

Clearly, this is not a good approximation for even times well within the linear regime. Recall that we are operating at $.01t_o$, where t_o is the temporal boundary between the linear and nonlinear regimes. Recalling the development of the nonlinear equations at the end of chapter II, the motivation for the approximation becomes clearer. Bryskin desired a form that would lend itself to analytic solution when determining the forms of the electric field at the illuminated face of the crystal and the location of the interface, z_o.

For the case where the absorption coefficient is large,

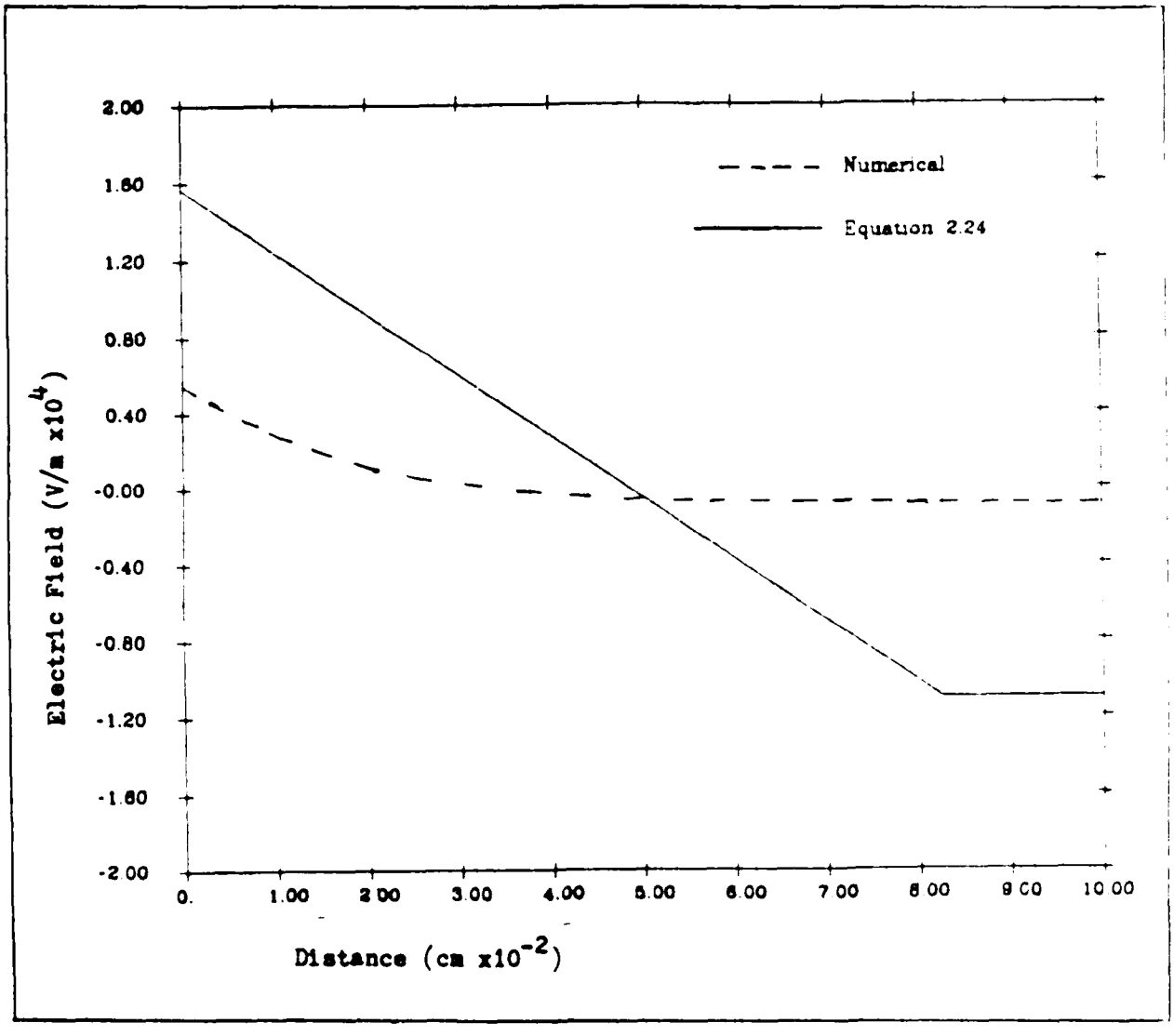

Figure 3.8. Linear Regime, Longitudinal Self Electric Field for $\alpha = 0.6\ cm^{-1}$, $t = .01t_o$

no approximation for the space charge density is given. The comparison between the analytic form of the space charge density and the numerical solution of space charge density is shown in Figure 3.3.

The approximate form of the electric field in the case where α is large is given in equation 2.25. Since equation 2.25 is very similar to equation 2.22, the difference between the value of the electric field at the illuminated face of the crystal for the approximate solution and the numerical solution should be very close to the difference found between the numerical and analytic cases. For large α, using α_3 as large α, the difference is 18.0%. Figure 3.9 shows the numerical and approximate solution for a large absorption coefficient.

Nonlinear Regime

For times greater than t_o, we can no longer approximate the electric field by E_o. The nonlinear section in Chapter II developed solutions for the electric field at the illuminated face of the crystal and the location of the interface, z_o, under the assumption of a small absorption coefficient. Therefore, we would not expect these results to hold for large absorption coefficients. It is also useful to remember that the approximation used for the charge number density 2.23 over predicted the total Q of the crystal by a factor of 4.8. So even in the case where the

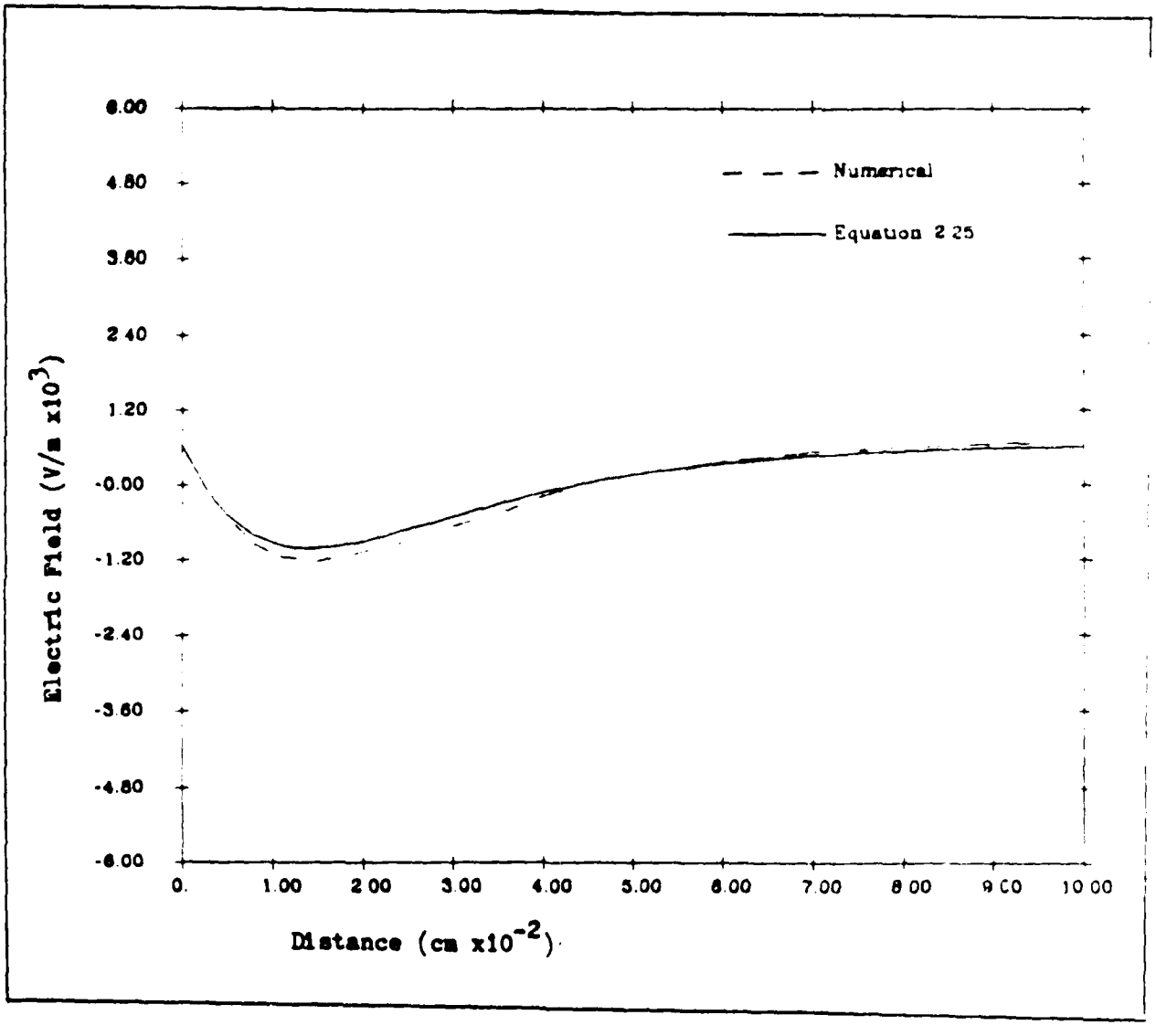

Figure 3.9. Linear Regime, Longitudinal Self Electric Field for $\alpha = 90\ cm^{-1}$, $t = .01t_o$

absorption coefficient is small, the prediction of the electric field at the illuminated face and the location of the charge interface could be seriously in error. The predictions are more useful for the predictions of the time dependences of the parameters.

The electric field at the illuminated face of the crystal for both the approximate and the numerical solution, is shown in Figure 3.10 for times $t > 1.5t_o$, and where α is small, $\alpha_1 = 0.6$. The results of equation 2.36 are approximately a factor of 1.5 greater than the numerical results. This is better than we anticipated in view of the comparison of predicted surface charge number, Q. The temporal correlation exhibits a dependence of $t^{0.74}$, in contrast with the analytic result of $t^{0.5}$.

Figure 3.11 shows the electric field at the illuminated face of the crystal for both the approximate and the numerical solution for the same time as Figure 3.10 but with $\alpha_3 = 90.0$. Notice that equation 2.36 does not depend on the absorption coefficient. Thus the results of equation 2.36 are approximately a factor of 7.0 larger than the numerical solution. The time dependence of the numerical solution is now $t^{0.21}$. The fit for both the magnitude of the field and the time dependence of the field exhibit poor agreement. This is to be expected because 1) in all cases the approximation from which the nonlinear results derived, equation 2.23, overestimates the charge present in the

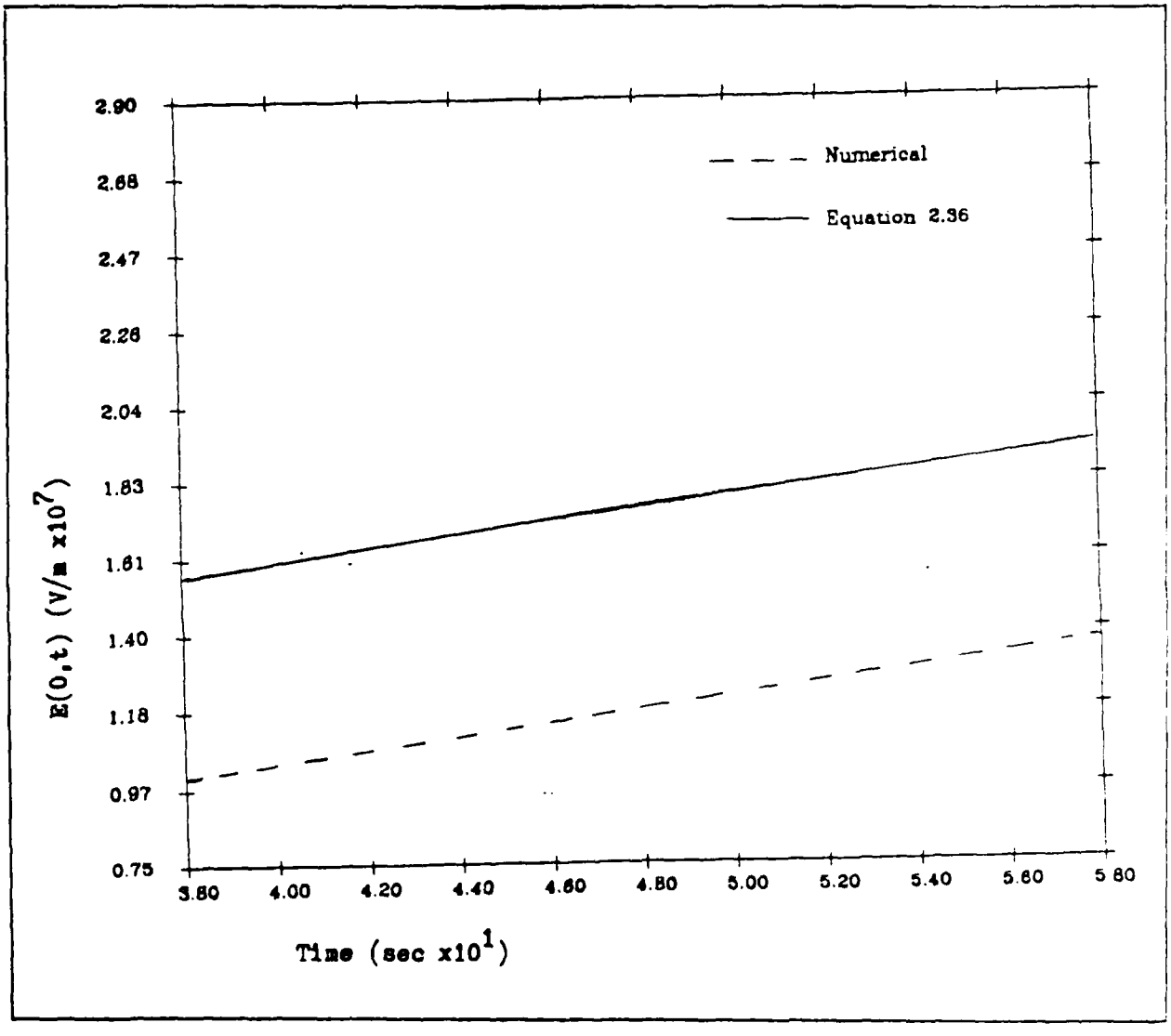

Figure 3.10. Nonlinear Regime, Magnitude of $|E(0,t)|$ with respect to time for $\alpha = 0.6$ cm^{-1}

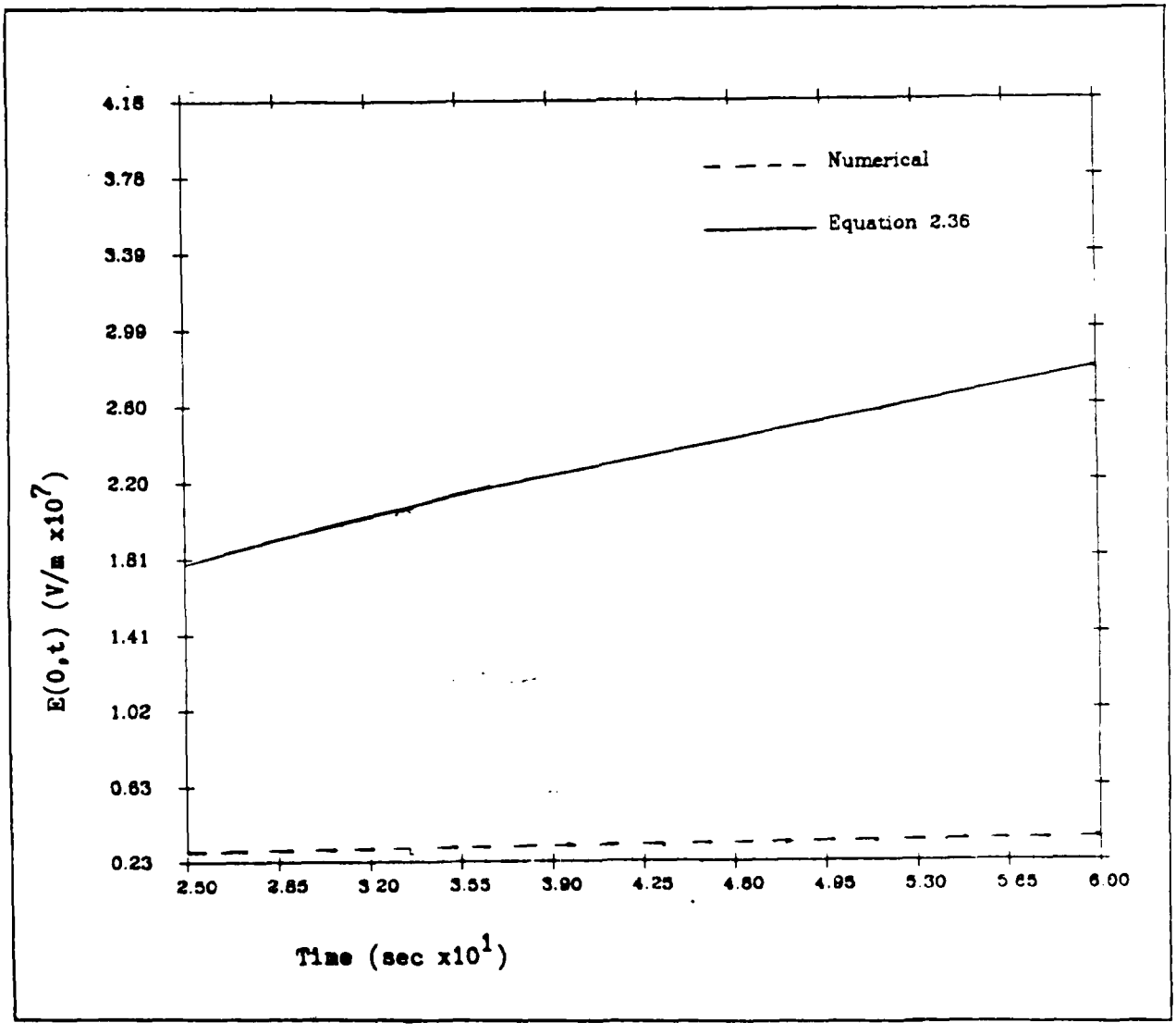

Figure 3.11. Nonlinear Regime, Magnitude of $|E(0,t)|$ with respect to time for α = 90 cm^{-1}

crystal; and 2) the absorption coefficient was assumed to be small throughout the derivation of the nonlinear results. The PRIZ write beam, however, is usually of such a wavelength so as to cause the absorption coefficient to be large. In addition, the beam is usually intense enough to cause the device to quickly enter the nonlinear regime. Thus, for most real applications of the device, only the numerical solution will suffice.

The approximate, equation 2.35, and numerical solutions for the location of z_o at various times when the absorption coefficient is small, α_1, are presented in Figure 3.12. The numerical results exhibit a dependence of $t^{-.555}$, which compares favorably with the analytically predicted $t^{-0.5}$ dependence. The analytic expression predicts the value of z_o to be approximately 0.8 of the numerical solution.

A similar comparison, now with a large absorption coefficient, α_3, is presented in Figure 3.13. The numerical data yields a dependence of $t^{-0.552}$, for $t > 1.5t_o$. Bryskins' value of z_o is roughly 2.0 times as far away from the illuminated face as the numerical prediction. The disparity in the location of z_o is expected, since Bryskins' derivation assumed that the absorption coefficient was small. The agreement in the time dependence of z_o is somewhat surprising.

We have seen that when $t << t_o$, the analytic expressions for the charge number density, equation 2.18,

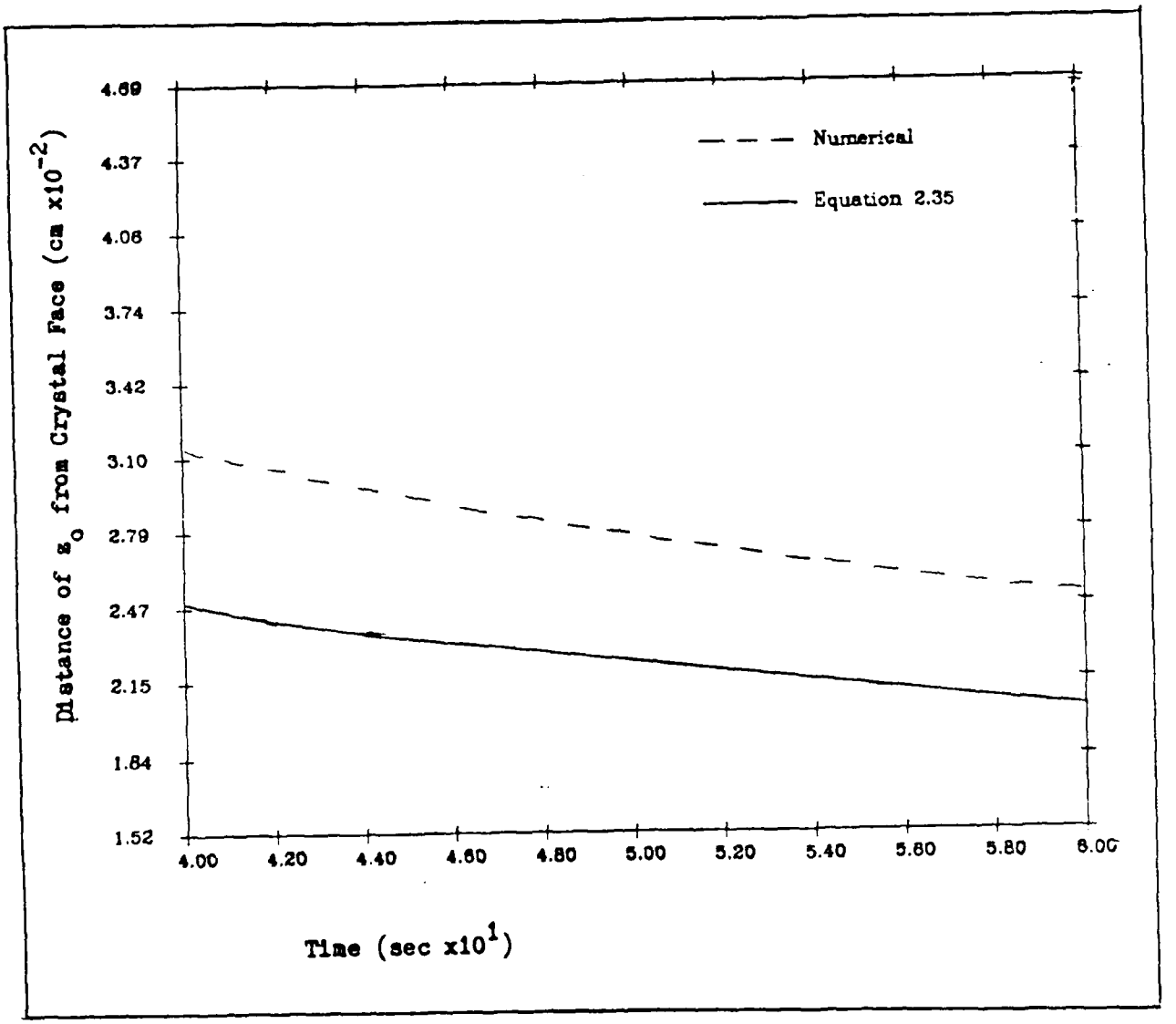

Figure 3.12. Nonlinear Regime, Location of Charge Interface, z_o, with respect to time for α = 0.6 cm^{-1}

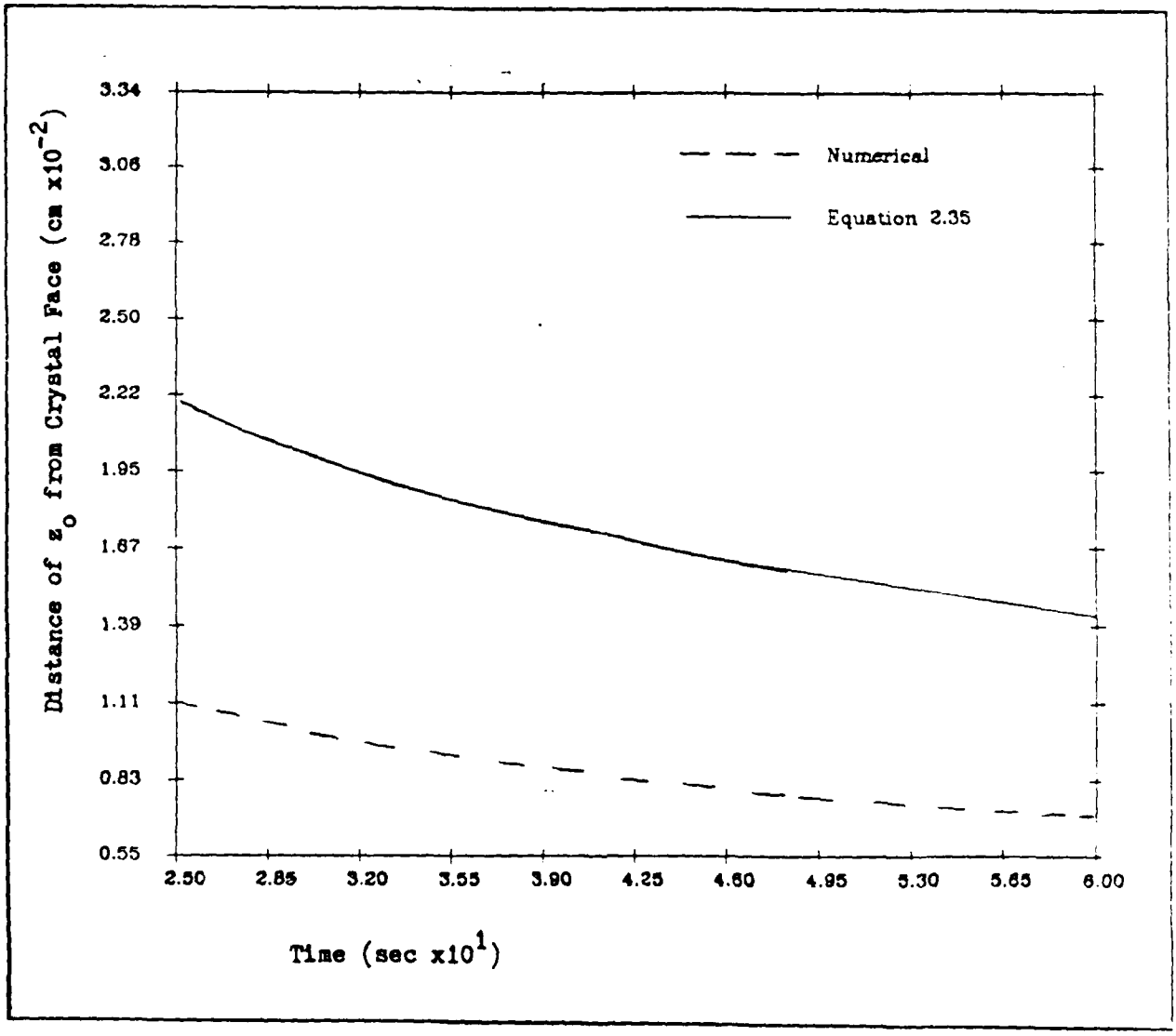

Figure 3.13. Nonlinear Regime, Location of Charge Interface, z_o, with respect to time for α = 90 cm^{-1}

the surface charge number density, equation 3.9, and the electric field, equation 2.22, exhibit excellent agreement with the numerical results. This agreement holds regardless of the absorption coefficient of the material for the wavelength under consideration. When $t > t_o$, the analytic expression for the charge interface, equation 2.35, exhibits acceptable agreement for all absorption coefficients. The expression for the electric field at the face of the crystal, equation 2.36, is only useful when the absorption coefficient is small.

Chapter IV

In the previous chapter the numerical model of the PRIZ was developed and validated using analytical results. It is more difficult to evaluate the model when considering experimental results. Soviet data on the longitudinal electric field exists. However, these data omit critical parameters that the numerical model requires for input. Using best estimates for these parameters, a comparison is undertaken, with any assumptions made clearly detailed.

Two interesting experimental observations relating to PRIZ operating characteristics are reported by Shields (ref. 17) and by Anderson (ref. 1 and ref. 2). Shields reports on the "edge enhancement" of a simple spot. The charge distribution provided by the numerical model are used to calculate the transverse fields in this simple case, and the result is related to Shields' observations. Anderson has reported that the BSO crystal suffers damage when operating in the dynamic imaging mode. Observations from the model will be offered to help explain this phenomenon.

Comparison of Model with Experiment

Bryskin offers experimental results in two papers, (ref. 6 and ref. 8). These results take on the form of the spatial dependence of the longitudinal field for a given set of parameters. Unfortunately, Bryskin does not

completely specify his operating conditions.

The results reported in ref. 6 are compared with the numerical model in Figure 4.1. The total exposure was not reported, nor was the time at which the measurements were taken. However, it can be assumed that as long as the same total energy is deposited on the PRIZ, the write time should be immaterial to the shape of the longitudinal electric field. Curve 1 has an applied field of 1.3×10^6 V/m and curve 2 has an applied field of 3.2×10^6 V/m. The power of the write beam at 441 nm was assumed to be 1.11 $\mu W/cm^2$ and the time of best fit was observed to be 4.0 seconds, for a deposition of 4.44 $\mu J/cm^2$. The greatest disparity can be seen in the electric field behavior beyond the bottleneck. For curve 1, the numerical result predicts a slight rise in the magnitude of the electric field, while the experimental data do not reflect this. For curve 2, the rise predicted by the numerical result is matched by the experimental data, although the magnitude of the rise for the experimental data is less than the rise in the numerical data.

Figure 4.2 shows the results reported in ref. 8 compared with the numerical model. The write intensity was again not specified in this model, but the time of the measurement was, therefore, once a reasonable match was achieved for a given excitation rate, g(0), the power of the write beam at 589 nm could be calculated to be 374 $\mu W/cm^2$, from equation 2.14. It should be noted that unlike in Figure

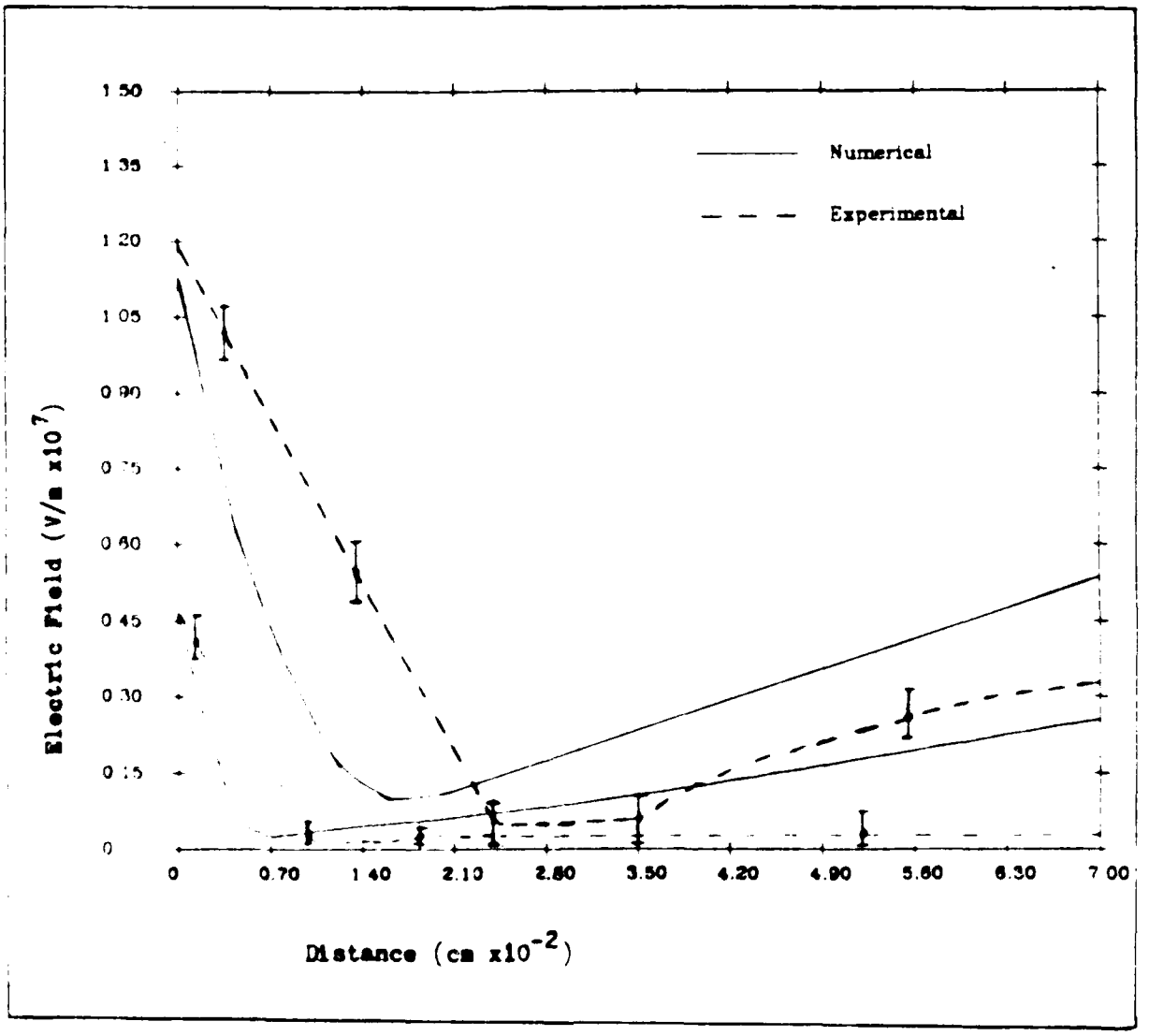

Figure 4.1. Longitudinal Electric Field, Numerical vs. Experimental (6:1687)

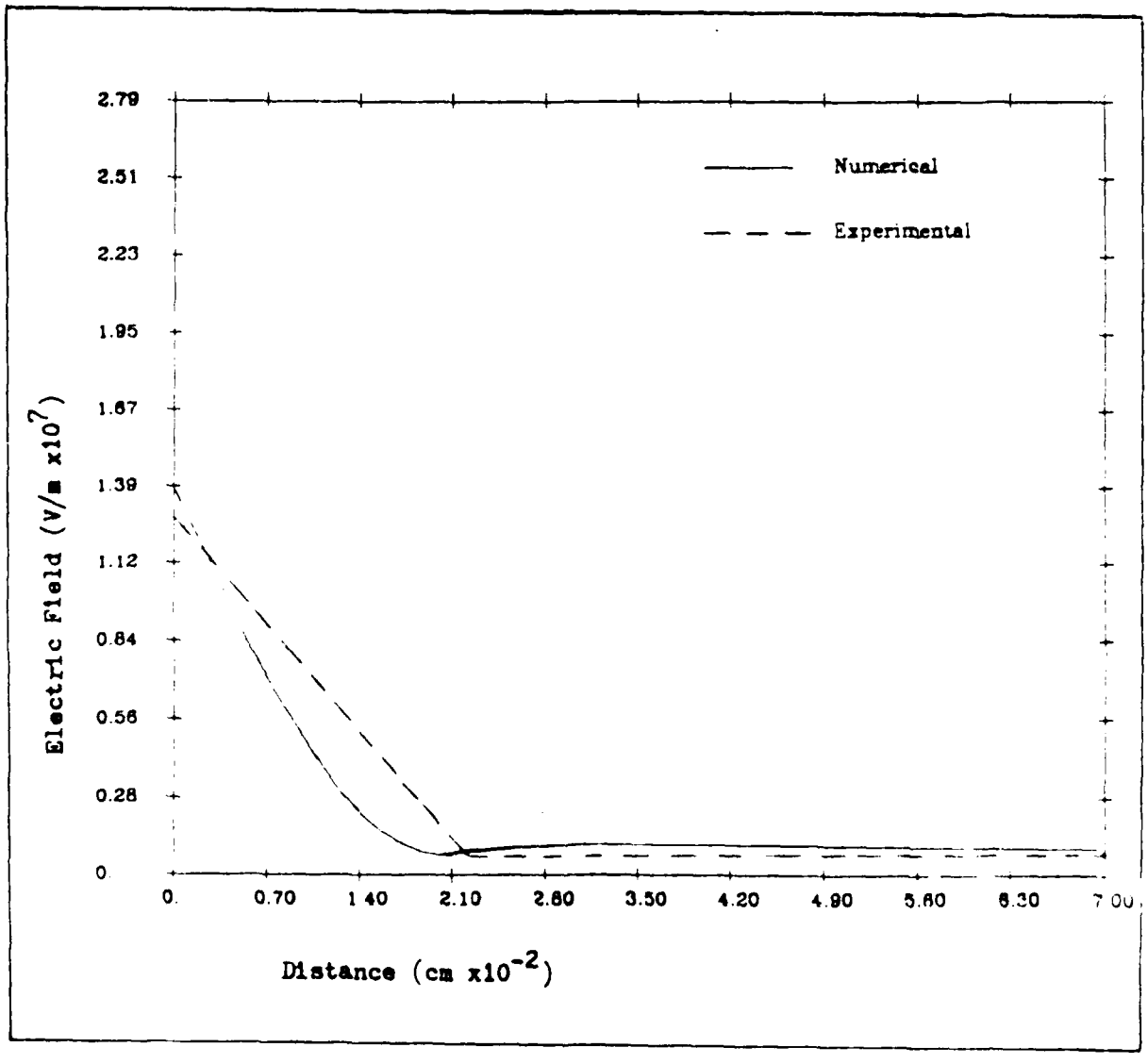

Figure 4.2. Longitudinal Electric Field, Numerical vs. Experimental (8:687)

4.1, where the quantum efficiency was 1.0 and the absorption coefficient 41.0 cm^{-1}, the quantum efficiency in Figure 4.2 was 0.03 and the absorption coefficient 0.6 cm^{-1}. So while almost all of the energy was absorbed in the experiment represented by Figure 4.1, very little of the energy was actually absorbed by the crystal in the experiment in Figure 4.2. In Figure 4.2 the agreement between experiment and the numerical model is much closer throughout the crystal than it was for Figure 4.1. The possible exception is the value of the field at the illuminated face of the crystal.

For these two cases, the numerical model was easily able to match the experimental results to within a factor of two. Thus the model should prove valuable as a tool for experimenters in developing further experiments dealing with the PRIZ device.

The Case of a Simple Spot

In the first chapter, an expression for the phase difference of the PRIZ crystal was developed, equation 1.1. This expression was dependent on the integrated transverse electric field. Up to now, we have been exploring solutions for the longitudinal space charge density and the longitudinal electric field. It was necessary to consider these together since they represent a coupled system. Now that we know the space charge density, we may now find the integrated transverse field for a simple case.

Method of Solution for a Simple Spot

The case to be treated is a circular write beam of small radius illuminating a spot on the crystal and generating a cylindrical charge distribution within the device. From this cylinder of charge, equipotential surfaces in the radial direction are calculated. The equipotential surfaces are approximated by treating the cylinder of charge as a set of discrete point charges and solving for the potential at discrete points in the radial plane. Thus in this solution, at any given point in the potential matrix, the potential contributions from the m discrete points in the longitudinal cylinder must be summed.

Once the numerical representation of the potential due to the charged cylinder is found, the transverse electric field is found by numerically approximating the differential between points in the potential matrix. This gives us a field

$$E_t = \frac{\partial \varphi}{\partial y} = \frac{\Delta \varphi}{\Delta y} = \frac{\varphi_j - \varphi_{j-1}}{y_j - y_{j-1}} \qquad (4.1)$$

where E_t is the transverse electric field at point j, and φ is the potential at the given point. The effect of the transverse field on the electrons in the conduction band is ignored. Further, in this case, the write beam is

considered to have a very small radius, on the order of 1 μm, and all calculations are made outside the radius of the beam. Hence, no effort was made to model the transverse electric fields in the actual write beam as it passes through the crystal. Since for equation 1.1 we need to know the integrated value of transverse field, the transverse fields at every given radial distance y from the write beam are integrated along the longitudinal axis.

Results in the Case of the Simple Spot

Figure 4.3 is a representative example of the equipotentials due to the write beam inside the crystal. The closely spaced lines show the concentration of positive charge near the illuminated face of the crystal. From this equipotential we can find the transverse fields at the discrete points for which the potentials are known. Figure 4.4 is a representative example of the transverse fields in the crystal. The horizontal axis of the figure labeled longitudinal axis is the direction parallel to the write beam. The vertical axis is the magnitude and direction of the transverse field at that radial distance. The axis facing more or less out of the page is the radial distance from the beam. Figure 4.4 shows that the largest magnitude of the field occurs closest to the beam and is generated by the large concentration of positive charge near the illuminated face of the crystal.

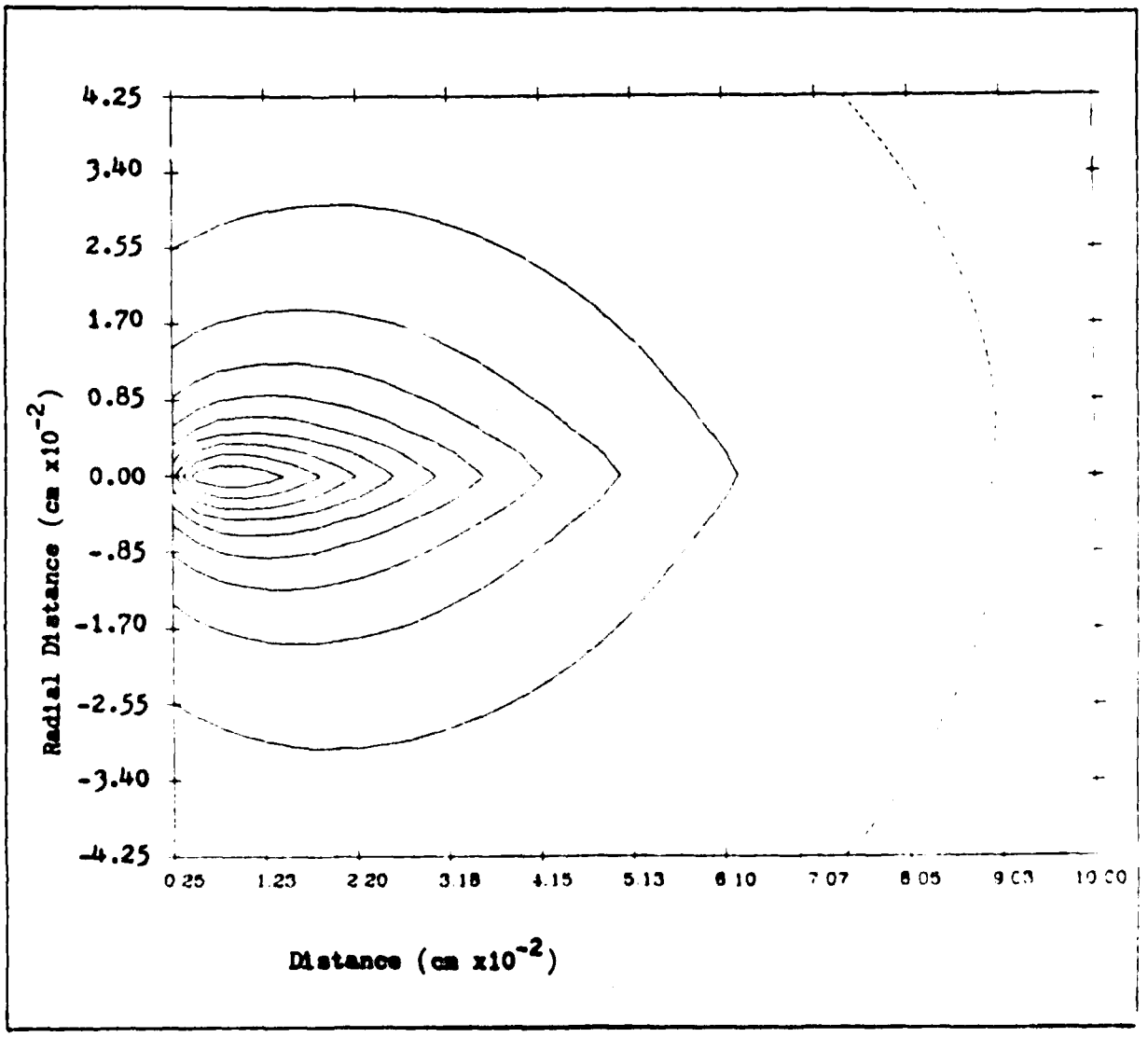

Figure 4.3. Equipotentials for a Small Circular Write Beam

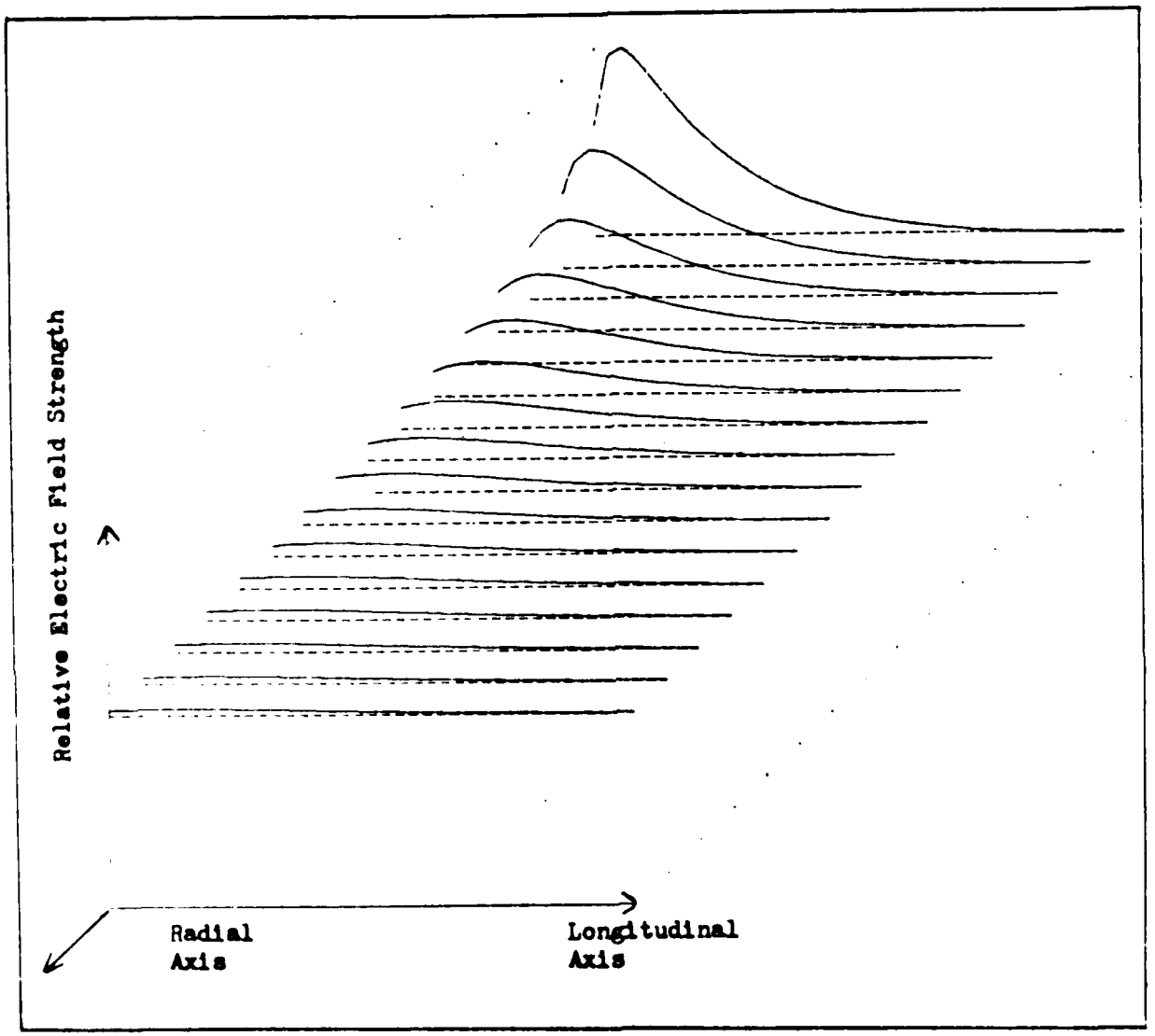

Figure 4.4. Transverse Electric Fields for a Small Circular Write Beam

In order to find the integrated value of the transverse fields in the longitudinal direction, each of the curves representing the magnitude and direction of the transverse field at a fixed radial distance along the longitudinal axis of beam is integrated. Figure 4.5 displays the results of this integration by examining the integral value with respect to radial distance from the beam. The dotted line present in the graph represents a strict y^{-1} dependence. To a reasonable approximation then, we see that the magnitude of the integrated value of the beam has an approximately inverse relationship with the radial distance from the beam.

Shields reports what he calls the "Edge-Enhanced Output Image of Input Spot" (17:22). The results shown in Figure 4.5 would indicate that we would find the largest value of the integrated transverse field, E_t', at or near the edge of the spot. From equation 1.1 the value of E_t' can be seen to be directly proportional to the phase difference. Since r_{63} is always a very small number the phase difference will most likely never exceed $\pi/2$, so an increase in the value of E_t'would bring about an increase in the intensity. So the edge-enhancement is something we would expect.

BSO Crystal Damage

Anderson reported damage occurring to the BSO crystal when the crystal is operated in the dynamic imaging mode. O'Dwyer (ref. 13) reports on the strength of electric field

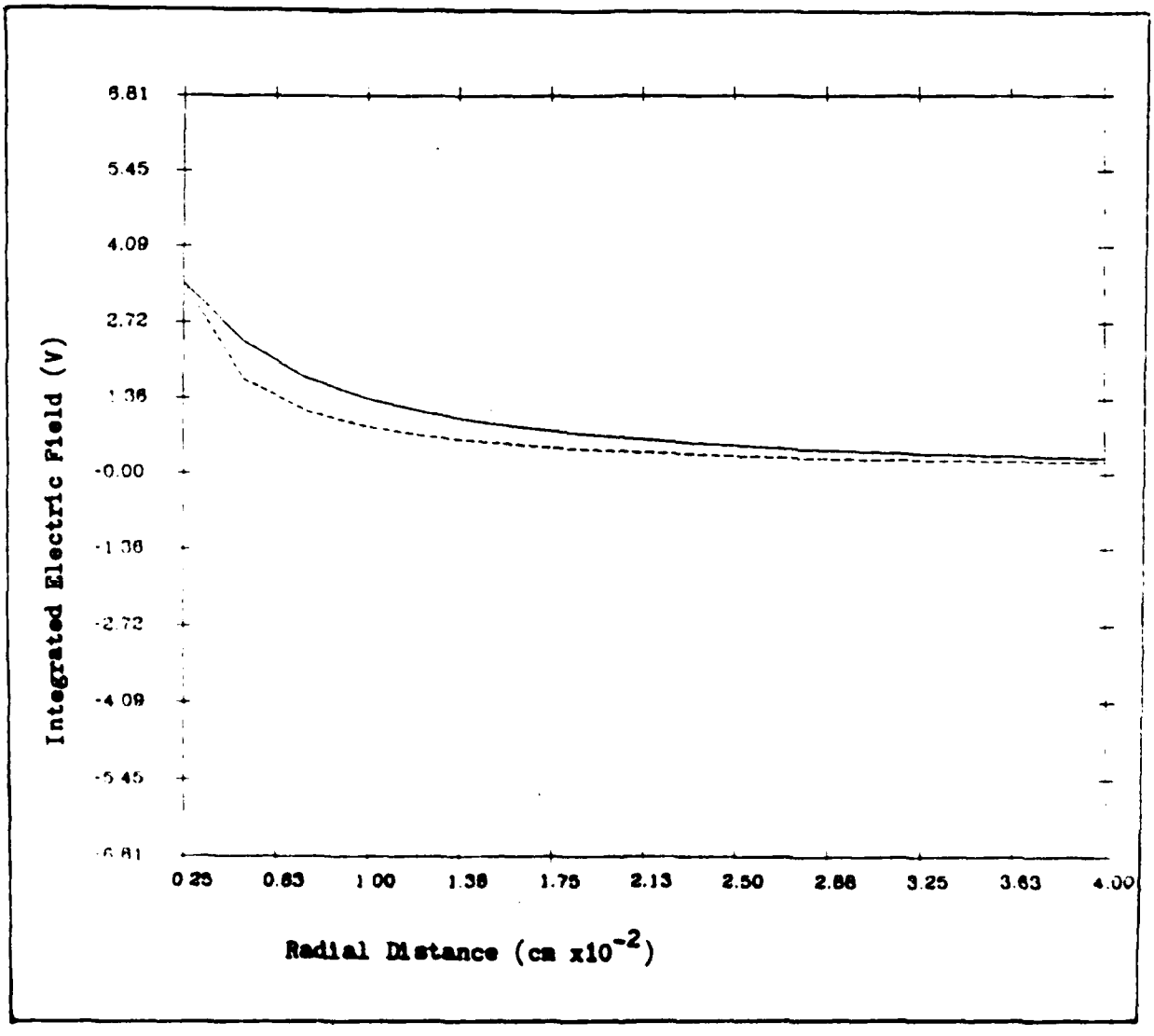

Figure 4.5. Integrated Transverse Electric Field for a Small Circular Write Beam

necessary to cause breakdown in various substances. Almost all of his results fall into the range of MV/cm or 10^8 V/m. We will accept this figure as a reasonable order of magnitude estimate for the field required to cause breakdown in a BSO crystal. Looking back at Figure 4.1, which corresponds to a write beam at wavelength 441 nm, we can compare with some of Andersons results, which were obtained with a 442 nm laser source.

For a write beam of 1.11 $\mu W/cm^2$, after 4 seconds the electric field at the illuminated face of the crystal has risen to 4.7×10^6 V/m. Increasing the write beam power density by a factor of 10 produces an electric field at the illuminated face of the crystal of 2.8×10^7 V/m. In his initial examination of damage to the PRIZ crystal, Anderson uses as his lowest write power 293 $\mu W/cm^2$ (1:4.5). It is easy to see that a write power of 293 $\mu W/cm^2$ could produce a field at the illuminated face in the range of 10^8 V/m. Thus it is highly likely that the observed damage resulted from breakdown in the vicinity of the illuminated surface.

Chapter V

Summary

The PRIZ operates by creating a phase difference between the indices of refraction perpendicular to the axis of propagation of the write and read beams. This phase difference can be calculated and is found to be proportional to the strength of the transverse electric field. This field arises from a space charge generated within the crystal. Thus, establishing the distribution of the space charge is a principal goal.

This study presents a review of the theory governing the excitation, charge transport and trapping of charge within the crystal. The theory is all based on the simplified system presented in equations 2.6-8. A qualitative discussion of the processes is presented. Two operating regimes, linear and nonlinear, were identified.

The theory for the linear regime has been fairly well established by Bryskin, but the opportunity was taken here to do more rigorous calculations to arrive at complete solutions for the longitudinal characteristics of the device. The numerical method used in solving the simplified system of coupled, first-order, differential equations is presented, and found to agree quite well with theory in the linear regime.

Bryskin has also developed a theory, albeit less

complete, for the nonlinear regime of the device. This theory is based on simplifying assumptions which severely limit the quantitative and even qualitative utility of the results. No analytical extensions of the theory in this regime was attempted in this study. The numerical solution is capable of operating quit well in either regime.

Experimental results reported in the literature are troubled by the omission of several important parameters in the presentation of the data. The experimental data which is presented is compared with numerical results, the assumptions made in the model in order to complete the parameter set are clearly laid out. Qualitative results are all in agreement. Some of the qualitative observations reported and confirmed by the numerical solution are:

1. The longitudinal electric field at the face of the crystal increases with time as the device is written upon.
2. The longitudinal electric field develops a bottleneck in the crystal which slows the escape of charge from the device.

Shields reports the edge enhancement of a simple spot. The numerical solution predicts the integrated transverse field at the edge of the spot to be a maximum. It also predicts the essentially $1/r$ fall off of that field.

Anderson (ref. 1 and 2) has studied the damage to the BSO crystal when operating in the dynamic imaging

The postulated mechanism leading to the damage is suspected to be dielectric breakdown. Using representative results taken from O'Dwyer (ref. 13), the numerical model shows that large write beam powers can create an electric field at the illuminated face of the crystal which is large enough to cause breakdown.

Recommendations for Further Research

Although the PRIZ was the device of primary interest in this study, the differential equations representing the charge transport in the BSO crystal are general. The method of solution of this system could be extended to other devices relying on internal charge distributions to generate longitudinal or transverse fields.

Grycewicz (9:1347) has proposed using the PRIZ for image selection and Nilius (ref. 12) has examined the long term memory of the device. Both of these uses depend on the time required for optical erasure. Therefore, it is important that the mechanism causing optical erasure be understood. Nilius reported the decay time of the image, τ_d, was related to the incident power on the crystal by the following empirical relation (12:34):

$$\tau_d = \frac{b}{I \Delta t} \qquad (5.1)$$

where I is the power per unit area, Δt is the duration of the write pulse, and b is a proportionality constant. Thus the memory time of the device is inversely proportional to the incident energy.

In the majority of this study it was assumed that the injection current across the illuminated face was zero. In selective tests, the boundary condition was modified to allow all of the charge escaping through the dark face to re-enter through the illuminated face. This is equivalent to assuming the barrier potential equal to zero. When this was done in the simple case of the spot, the magnitude of the integrated transverse electric field was seen to drop by at least three orders of magnitude. This suggests that the injection current is a major contributor to the optical erasure.

If we assume a barrier potential at the illuminated face, we would expect a large magnitude electric field at the illuminated face to cause a larger injection current than a smaller magnitude field. Thus, the larger the value of the electric field at the crystal, the shorter the lifetime of the image. The strength of the field at the illuminated face of the crystal is proportional to the total charge contained within the crystal. The rate of formation of total charge is proportional to the intensity of the write beam. The higher the intensity of the write beam, the larger the magnitude of the electric field at the

illuminated face of the crystal, and the shorter the decay time of the image, t_d.

This suggests two areas of further research. One is the more accurate modeling of the injection current. This will involve research into the nature of the barrier potential at the illuminated face of the crystal. The second area of research is in the area of increasing the memory time of the PRIZ. Both theoretical and experimental work should be pursued with a "semi-conducting" PRIZ, where the charge is allowed to escape freely from the dark face of the crystal, and a dielectric is used to prevent electrons from entering the illuminated face of the crystal. It is postulated that significant memory times could be achieved even with fairly strong write beams in this manner.

The only solution to the actual integrated transverse field presented in this study is the case of a simple spot. In addition, the transverse field internal to the write beam is neglected. More work on the solution to the transverse field in more complex cases is needed, in addition to modeling the fields effects on the electrons in the conduction band. A good starting point, using the charge distribution generated in this study, would be to modify the results of Owechko and Tanguay (ref. 14) to model much more complex images.

Bibliography

1. Anderson, 1Lt Danny L. Analysis of Write-Beam-Induced Damage on the Conducting PRIZ. MS Thesis, GEP 86D-1, School of Engineering, Air Force Institute of Technology (AU), Wright-Patterson AFB, OH, 45433, (December 1986).

2. Anderson, 1Lt D. L. and Luke, T. E. Write-Beam Induced Crystal Damage in the Conducting PRIZ. Paper Submitted for Publication, Air Force Institute of Technology (AU), Wright-Patterson AFB, OH, 45433.

3. Astratov, V. N. et al. "Dynamics of the Distribution of the Field and Charge in $Bi_{12}GeO_{20}$ in the Case of Thermal Ionization of Traps," Soviet Physics Solid State, 25 (9): 1585-1587 (September 1983).

4. Boas, M. L. Mathematical Methods in the Physical Sciences. New York: John Wiley and Sons, 1983.

5. Bryskin, V. V. et al. "Dynamics of Optical Charge Formation in Crystals with the aid of the Internal Transverse Pockels Effect," Soviet Physics Solid State, 24 (1): 82-86 (January 1982).

6. Bryskin, V. V. et al. "Initial Stage in the Redistribution of Photoinduced Charges and Electric Fields in $Bi_{12}SiO_{20}$," Soviet Physics Solid State, 24 (10): 1686-1689 (October 1982).

7. Bryskin, V. V. and Korovin, L. I. "Nonlinear Theory of the Distribution of an Electric Field in Photorefractive Crystals," Soviet Physics Solid State, 25 (1): 30-33 (January 1983).

8. Bryskin, V. V. et al. "Effect of Light Absorption on the Electric Field Distribution in $Bi_{12}SiO_{20}$," Soviet Physics Technical Physics, 9 (6): 686-689 (June 1983).

9. Bryskin, V. V. and Korovin, L. I. "Role of Injection Currents in Dynamic Image Selection Under Conditions Nonlinear in the Electric Field," Soviet Physics Solid State, 25 (8): 1347-1351 (August 1983).

10. Bryskin, V. V. et al. "Linear Operation of PRIZ Space-time Light Modulators," Soviet Physics Technical Physics, 29 (8): 878-882 (August 1984).

11. Gear, C. W. Numerical Initial Value Problems in Ordinary Differential Equations. New Jersey: Prentice Hall, Inc., 1971.

12. Nilius, Maj Mark E. Measurement and Analysis of the Memory Capabilities of a Conducting PRIZ. MS Thesis, GEO 85D-3, School of Engineering, Air Force Institute of Technology (AU), Wright-Patterson AFB, OH, 45433, (December 1985).

13. O'Dwyer, J. J. The Theory of Dielectric Breakdown of Solids. Oxford, Clarendon Press, 1964.

14. Owechko, Y. and A. R. Tanguay, Jr. "Theoretical Resolution Limitations of Electrooptic Spatial Light Modulators. I. Fundamental Considerations and II. Effects of Crystallographic Orientation," Optical Society of America, 1 (6): 635-652 (June 1984)

15. Peltier, M. and Micheron, F. "Volume Hologram Recording and Charge Transfer Process in $Bi_{12}SiO_{20}$ and $Bi_{12}GeO_{20}$," Journal of Applied Physics, 48 (9): 3686-3690 (September 1977).

16. Petrov, M. P. et al. "The PRIZ Image Converter and its use in Optical Data Processing Systems," Soviet Physics Technical Physics, 26 (7): 816-820 (July 1981).

17. Shields, Capt. Duncan M. Construction and Analysis of a PRIZ Spatial Light Modulator Exhibiting Dynamic Image Selection. MS Thesis GEO 84D-4, School of Engineering, Air Force Institute of Technology (AU), Wright-Patterson AFB, OH, 45433 (December 1984)

VITA

First Lieutenant David A. Cushing was born 5 March 1961 in Casper, Wyoming. He graduated from high school in Englewood, CO in 1979. He earned his Bachelor of Science degree in Physics at Colorado State University. Upon graduation, in December 1983, he was commissioned a Second Lieutenant in the Air Force through ROTC. His first assignment was at the Foreign Technology Division, Wright-Patterson AFB, OH. He served as a Space Systems Analyst in the Sensor Data Directorate. In May 1986, he entered the School of Engineering, Air Force Institute of Technology, as a Master of Science degree candidate in Engineering Physics.

Permanent Address: 5801 Lowell NE, Unit 25-D
Albuquerque, NM 87111

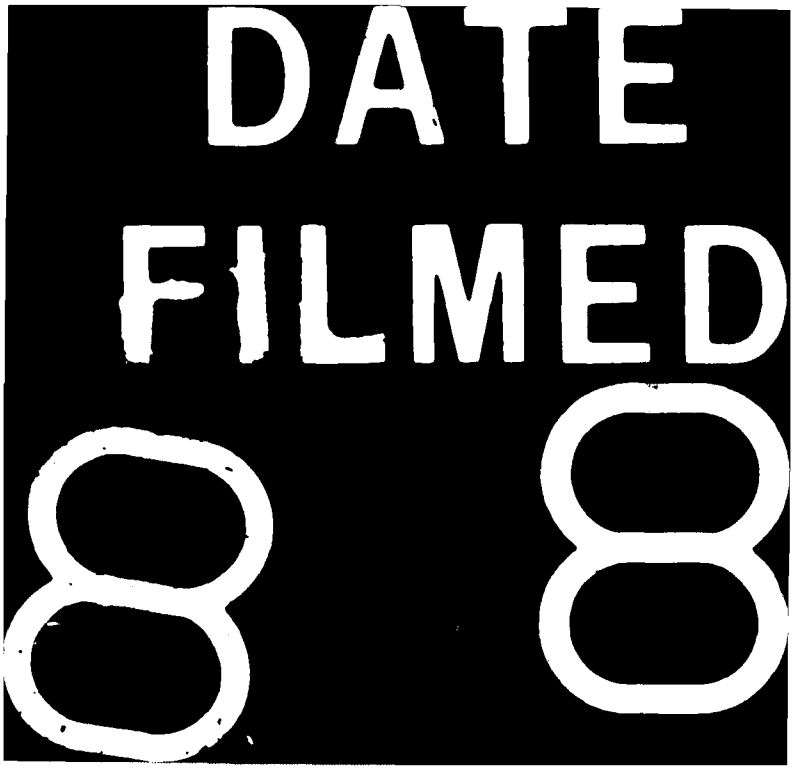
DATE
FILMED
8 8